Arabian Journal of Chemistry (2022) **15**, 104025

King Saud University

Arabian Journal of Chemistry

www.ksu.edu.sa
www.sciencedirect.com

ORIGINAL ARTICLE

Modelling and optimization of crude oil removal from surface water via organic acid functionalized biomass using machine learning approach

Christian O. Asadu [a,*], Benjamin Nnamdi Ekwueme [b], Chijioke Elijah Onu [c], Thomas O. Onah [d], Innocent Sunday Ike [e,f], Chinonso Anthony Ezema [g,h]

[a] *Department of Chemical Engineering, Gregory University, P.M.B 1012, Uturu Abia State, Nigeria*
[b] *Department of Civil Engineering, Faculty of Engineering, University of Nigeria, Nsukka Enugu State, Nigeria*
[c] *Department of Chemical Engineering, Nnamdi Azikiwe University, Awka, Nigeria*
[d] *Department of Mechanical Engineering, Enugu State University of Science and Technology, Enugu, Nigeria*
[e] *Deaprtment of Chemical Engineering, Federal University of Technology, Owerri Imo State, Nigeria*
[f] *African Centre of Excellence in Future Energies and Electrochemical System (ACE-FUELS), Federal University of Technology, Owerri, Nigeria*
[g] *Department of Microbiology, University of Nigeria Nsukka, Enugu State, Nigeria*
[h] *Graduate School of Life Science, Hokkaido University, 060-0810 Sapporo, Japan*

Received 13 February 2022; accepted 29 May 2022
Available online 2 June 2022

KEYWORDS

Crude oil;
Modelling;
Banana peels fiber;
Optimization;
Adsorption

Abstract Banana peel fiber adsorbent (BPF) with well-arranged substructure of pores was fabricated via esterification reaction with organic acid and biomass. The emerged adsorbent (BPF) was employed in taking away crude oil from water surface. Three machine learning tools such as RSM, ANN and ANFIS was employed for the modelling and optimization of the process. From results, the optimal oil layer removal of 98.2% was achieved at oil water ratio of 0.2 g /100 cm^3. For now, BPF displayed high adsorptive prospect at a very low pH of 4 with 96.8% oil removal. On the other hand, the activation energy, enthalpy change and entropy change of the system are (18.56, 25.44, −0.751 KJ/mols) and (25.77, 29.16, −0.813 KJ/mols) designating a non-spontaneous system. The process of removal by BPF really matched the Langmuir isotherm model as proved by statistical error analysis with highest adsorption capacity of 49.33 mg/g as shown through equilibrium modeling. RSM displayed the optimum conditions of the key variables such as temperature, oil concentration, adsorbent dosage, pH and time as 100 °C, 0.2 g/100 cm^3, 1.5 g, 2 and 75 mins, respectively. Analysis of the three generic algorithm indicated significant oil

* Corresponding author.
E-mail addresses: aasadu@yahoo.com, a.christian@gregoryuniversityuturu.edu.ng (C.O. Asadu).
Peer review under responsibility of King Saud University.

Production and hosting by Elsevier

https://doi.org/10.1016/j.arabjc.2022.104025

Nomenclature

RSM	Response Surface Methodology	SEM	Scanning Electron Microscope
ANN	Artificial neural network	FTIR	Fourier Transform Infrared Spectroscope
ANFIS	Adaptive neuro-fuzzy inference system	ANOVA	Analysis of Variance
CCD	Central Composite Design		
BPF	Banana Peels Fiber		

removal prediction with quite remarkably similar coefficient of correlation of 0.999. Additional statistical analysis suggested that RSM was marginally better than ANN and ANFIS for the modelling of crude oil removal via esterified banana peels fiber.

1. Introduction

If the degree of oil contamination of our environment mostly water bodies is not addressed urgently, there will be eminent impending food insecurity in Nigeria and the globe at large. Research has demonstrated that oil spill is greatly inimical to agricultural development and mitigates every effort as presented by Happi-Emaga et al., 2011. Nigerian Bureau of Statistics reported in 2020 that the amount of oil spill in Nigeria cannot is unquantifiable due to lack of correct/precise data (Reza et al., 2013). The environment of the Niger Delta region of Nigeria has not been green for many years now because of the consequences of oil pollution (Happi-Emaga et al., 2011; Reza et al., 2013; Annunciado et al., 2005). The exhaustion of oxygen and insufficiency of dissolved oxygen in water bodies because of oil spills have adversely affected the sustenance of oceanic fauna in this region of the globe (Annunciado et al., 2005; Behnood et al., 2013; Rahman et al., 2021a). The crude oil spillages have been attributed to underground pipe breakdown, crisis among the host settlements, tank accident, exploration, etc., (Happi-Emaga et al., 2011; Kharoune et al., 2001; Rahman et al., 2021b; Gwendoline,2010). Several groups have directed their attention to getting the most suitable and effective way to rectify the issue and upturn the impending food insecurity. Studies has been ongoing on various methods to address this crisis, such as chemical remediation (Awual et al., 2019a; Awual et al., 2019b), bioremediation (Kharoune et al., 2001; Kumar,2006; Ladhe et al., 2011), ultrafiltration (Nwabanne et al., 2018; Thompson et al., 2020) and other innovations on wastewater treatments like natural treatment and coagulation (Suidan et al., 2005; Ayotamuno et al., 2006; Yang et al., 2006). All these approaches appear to be economically infeasible (Happi-Emaga et al., 2011; Baars, 2002), demanding more studies on adsorption methods which have been generally adjudicated to be cheap, simpler and sustainable.

The scarcity and impractical cost of non-biodegradable traditional adsorbents for adsorption occasion for exploration of workable alternative. Employment of agro-industrial wastes for clean technology is really attracting great acceptance in most oil polluted region of the globe. Previously, other ways of crude oil remediation were employed but recently, group of researchers have move towards renewable and biodegradable materials in order to suppress the environmental crude oil pollution (Ogbodo et al., 2021; Asadu et al., 2021a; Asadu et al., 2021b). Thus, evolution development via research is inevitable. Again, the character of these agro-industrial wastes greatly depends on the origin and source as well as postharvest mechanism (Onwu et al., 2019a; Onwu et al., 2019b; Asadu et al., 2018). Consequently upon this, authors of this study concluded to move toward employing indigenous agro-industrial waste like banana peels fiber (BPF) as prospective adsorbent for reversing the crude oil damage. The wastes has high percentage of lignocellulosic materials containing cellulose, lignin, hemicellulose, etc., thus they are good materials for adsorbent fabrication. They also contain high amount of fiber which could be converted into various other functional materials (Vigneswaran et al., 2015; Okafor et al., 2012). This research has acquired many commendations because its introduction at a time the country has moved to agriculture as its major source of revenue generation.

Different groups have fabricated adsorbents from other agro-industrial wastes like groundnut shell (Happi-Emaga et al., 2011), wood (Albert et al., 2016), kola nut shell (Chinonye et al., 2018), and banana waste (Pelissari et al,2014). Consequently, this study focuses on examination of thermodynamics and optimization of process conditions of crude oil removal via fabrication of adsorbents from banana peels fiber (BPF).

Also, agro-industrial wastes are readily obtainable at no cost (Asadu et al., 2021a), are biodegradable and have been shown to be an effective adsorbent (Chinonye et al., 2018, though the changes in the activation approach is a source of concern. Some researchers employed mineral acids and alkalis that are harmful to the environment, thus generating more environmental issues when the adsorbents are discarded at the end. This is part of the gaps this study will bridge through use of organic acid such as stearic acid that are more human and environmentally friendly for activation the biomass.

Some works on the fabrication of adsorbent from Banana peels fiber for removal of various pollutants and heavy metals have been published, but none has reported its use as adsorbent for removal of crude oil layer from surface water. Other researchers have examined banana peels fiber as prospective raw materials for fabrication of fiber board, composite, paper production etc. (Alvarez-López et al., 2014), but its prospect as adsorbents is yet to be extensively examined. Therefore, bridging the aforementioned gap by fabricating alternative adsorbent from banana peel fiber is imperative.

Thus, this present work intends to (i) explore the prospect of fabrication of an acceptable adsorbent from Banana peels fiber for crude oil polluted water remediation. (ii) Examine the equilibrium and thermodynamics of the process and (iii) Optimize the key process parameters via response surface methodology, adaptive neuro-fuzzy inference system and artificial neural network modelling.

The application of thermodynamics and equilibrium in modeling was taken early on to the examination of chemical species and reactions (Egbuna et al., 2019a). Chemical thermodynamics examines the nature of the activities of entropy, enthalpy and free energy in chemical reactions or diffusion processes of molecules and has given the bulk of expansion and understanding of the field (Egbuna et al., 2019b). Nevertheless, thermodynamics and equilibrium modeling of removal of

crude oil from water surface has drawn reasonable attention of researchers worldwide due to the adverse effect of crude oil spills to our entire surroundings.

Modeling of the process variables can enhance the interactive effects of the variables while increasing the percentage of oil removal. Presently there is no report or any work on modelling and optimization of crude oil removal by activated BPF using machine learning approach. This present exercise also intends to employ response surface method (RSM), artificial neural network (ANN), and adaptive neuro fuzzy inference system (ANFIS) for the modelling and optimization. RSM can generate empirical model that can yield optimal response using minimal experimental data sets (Nwobasi et al., 2022; Onyekwelu et al., 2021; Ezedinma et al., 2021). ANN works on the principles of neural system to model complex nonlinear processes (Asadu et al., 2019; Elijah et al., 2020; Gholamhossein et al., 2016). ANFIS is a hybrid fuzzy and neural systems that efficiently models industrial processes with minimum error (Onu et al., 2021, 2022; Bahman and Sina, 2018). Optimization could be employed to minimize or maximize objective function (problem) subject to the certain constraints (Nnaemeka et al., 2021; Ezenwa et al., 2019; Ugwele et al., 2020). The optimization problems can be linear, geometric or even quadratic. The key reason for statistically developing a problem or perhaps an experiment is to combine the regular interface between different components that have effects on the method towards obtaining expected conditions. Statistical and mathematical tools like RSM and other approaches have been used to optimize adsorption variables in order to attain maximum removal efficiency (Rahman and Raheem, 2022).

2. Materials and method

2.1. Collection of samples, pretreatments and preparation

Banana peels fiber utilized in this study was sampled from local market in Enugu State Nigeria. Riped banana peels were size-reduced, cleaned with deionized water, thereafter dried under severe acute sun for seven days and oven dried at 120 °C for 20 h. It was further size-reduced to fine powder using grinder and sieved to particle size of 75 μm with aid of sieve net and was designated as BPF. The stearic acid, sulphuric acid (H_2SO_4) and caustic soda (NaOH) utilized in this study were purchased from major marketers in Enugu Nigeria and they were used without further purification.

2.2. Preparation of the organic acid functionalized biomass adsorbent (BPF)

The oven dried sample of BPF was subjected to thermal activity in a muffle furnace (model HCK 15/4 No: 20–40509, Taiwan) in the presence of ultra-high purity nitrogen (UHPN) atmosphere at a constant temperature of 500 °C for 8 h. BPF after heating was left standing for 1.40 min. 10 g of the carbonized samples were activated with 0.5 g of stearic acid in 200 ml of n-hexane that has two drops concentrated H_2SO_4 as catalyst. The mixture was refluxed in dean stark apparatus at 65 ± 1 °C for 2.5 h. The synthesized esterified acid–biomass at the end was severally cleaned with n- hexane. The samples were thereafter dried in oven again at 105 °C for 7 h and later stored in a tight polyethylene container. The sample variation in weight were determined via equation (1). The above procedure was according to method by Ogbodo et al., 2021 and Asadu et al., 2021a with slight modification.

$$\text{Percentage change in weight} = \frac{\text{Increase in weight}}{\text{Initial weight}} \times 100 \quad (1)$$

2.3. Determination of sample pH

15 g of BPF samples was boiled for 5 min in a beaker containing 150 ml of deionized water and thereafter allowed standing for further 10 min according to Onwu et al., 2019a. The mixture was then diluted to 200 ml and the pH determined thereafter. The pH was determined in triplicate and the mean value obtained and noted.

2.4. Treated and untreated BPF properties evaluation

The BPF properties assessment commenced with physical properties and then the instrumental characterization. American Society for Testing and Materials (ASTMD 5142, 3174, 872 and 3175 for moisture, ash, volatile and fixed carbon) (Ozçimen, 2012; Dil et al., 2019a) were utilized. The samples surface size or surface area was examined using the method described by Ogbodo et al., 2021. The method of Cadena et al. (2017) was used to assess the lignin and cellulose content of the fiber. Surface morphology was done with SEM (Model 302 Hitachi Japan) and FT-iR (Model 30LD, Hitachi, Japan).

2.5. General experimental procedure for oil layer removal by activated BPF

The experimental procedure used by Banerjee et al., 2006 was adopted with little modification. The experiment commenced with concentration of 100 mg/l of 100 ml crude oil–water mixture in a 200 ml beaker produced by mixing the oil and water at room temperature for 15 mins. A 0.3 g of the prepared BPF was added to the crude oil–water mixture and the resulted mixture separated after allowing it to stand for 75 mins at temperature interval of 20, 40, 60, 80 and 100 °C. The separation was achieved with a sieving net setting the pH at 7. The recovered BPF after separation was air dried and weighed and noted. The experiment was repeated using oil water concentration of 150, 200, 250, and 300 mg per liter. Amount of oil removed was obtained from weight after adsorption and pre-weight of the activated BPF. Equation (2) (Cheenmatchaya and Kungwakunakorn, 2014) was utilized in calculating the capacity of adsorption (qe) whereas the percentage removal was determined by equation (3).

$$\text{Capacity of adsorption process (qe)} = \frac{(\text{Co} - \text{Ce})}{\text{W}} \times \text{V} \quad (2)$$

$$\text{Quantity of oil recovered (\%)} = \frac{(\text{Co} - \text{Ce})}{\text{Co}} \times 100 \quad (3)$$

where;

C_o = Initial amount of oil (mg/l).
C_e = Quantity of oil at equilibrium (mg/l).
V = Volume of the oil–water mixture (ml).
W = Weight of BPF in grams.

2.6. Isotherm modeling of the oil layer removal using organic acid activated BPF

In order to forecast the model that most suitably describes the process of crude oil adsorption onto BPF in experiment 2.5, some of the picked models as presented in Table 1 were sufficiently studied (see Table 2).

2.7. The studies of the thermodynamics and activation energy of the process using BPF

Thermodynamics examination and assessment was performed to determine the enthalpy (ΔH), entropy (ΔS), and Gibb's free energy of activation (ΔG) for the sorption of oil onto the pores. These thermodynamic properties are important ingredients for explaining the behavior of adsorption process (Nwabanne et al., 2018). In order to determine these parameters, activation complex theory built by Eyring was helpful in assessing the thermodynamic parameters from temperature-dependent rate constants. Parameters determined from the Eyring-Polanyi equation (9) are comparable to the Arrhenius equation:

$$k = \frac{k_B T}{h} exp\left(-\frac{\Delta G}{RT}\right) \tag{9}$$

Substituting $\Delta H - T\Delta S$ for ΔG in equation (9), and taking natural logarithm gives equation (10):

$$In\left(\frac{k}{T}\right) = -\frac{\Delta H}{R}\left(\frac{1}{T}\right) + \left[In\left(\frac{k_B}{h}\right) + \frac{\Delta S}{R}\right] \tag{10}$$

where K is the rate constant at temperature T, ΔH and ΔS are the changes in enthalpy and entropy of activation for the reaction system, respectively. k_B and h are the Boltzmann (1.38×10^{-23} J K^{-1}) and Planck (6.63×10^{-34} Js) constants, while R stands for the universal gas constant. Equation (9) is comparable to Van't Hoff equation describing the mathematical relationship between enthalpy and entropy of activation with the rate constant. The plot of $\frac{1}{T}$ $vs. In(k/T)$ has the slope and intercept as $-\Delta H/R$ and $In(k_B/h) + \Delta S/R$, respectively. Also, the energy level of the molecules required to start a reaction or diffusion of molecules onto the surface of the microporous BPF is the activation energy. In a second order model, the rate constants grow with temperature and is explained by the Arrhenius law as shown in equation (11).

Table 1 Selected isotherm models examined.

Model	Equation	Equation number	Reference
Langmuir	$q_e = \frac{Q_m b C_e}{1+bC_e}$	(4)	(Paulauskiene et al., 2014)
Dubinin Radushkevich	$\ln q_e = \ln q_n - \beta_e^2 \varepsilon^2 = RT\ln(1 + 1/C_e)$	(5)	(Nestor et al., 2004)
Freundlich	$q_e = K_f C_e^{1/n}$	(6)	(Asadu et al., 2019)
Temkin	$q_e = \frac{RT}{b}\ln(ACe)$	(7)	(Olufemi et al., 2014)
Elovich	$In\frac{q_e}{C_e} = InK_e q_m - \frac{q_e}{q_m}$	(8)	(Thompson et al., 2020)

$$K = A\exp\left(\frac{-E_a}{RT}\right) \tag{11}$$

where K = is the adsorption rate constant (L g^{-1} min^{-1}).

A = is the temperature independent factor (L $g^{-1}min^{-1}$).
E_a = is the energy of activation (J mol^{-1}).
R = is the gas constant (8.314 J mol^{-1} K^{-1}).
T = is the absolute suspension temperature (K).

Linearization of equation (11) yields equation (12). The values of the activation energy (E_a) and the temperature independent factor (A) are determined from the slope and the intercept of the plot of Ln (K) against I/T, respectively.

$$\ln(K) = \ln(A) + \left(\frac{-E_a}{R}\right)\frac{1}{T} \tag{12}$$

2.8. Error analysis and Models' verification

To clearly predict the model of best fit as listed in Table 1, the performance of the isotherm models was subjected to further statistical analysis (see Table 2) so as to verify the importance of the models and rank them according to their performance. The relevant error functions used were given in equations (13) to (18). The statistical models gave an indication of how closely the predicted crude oil removal is to the experimental crude oil removal.

2.9. Optimization modelling using machine language RSM

The process of oil removal was optimized via Central Composite Design (CCD), a response surface methodology (RSM) with the capability to forecast second order or higher order models. This was performed in order to determine the optimum parameters or factors for oil removal with BPF. This also helps to investigate the communication influences of the five key factors. The independent parameters examined were temperature X_1(°C), Oil concentration X_2(g/100 cm^3), dosage. X_3(g), pH X4, and time X_5 (mins). These parameters were the independent factors whereas the percentage of oil adsorbed or removed (%R) were the dependent parameters or responses. The ranges of time, temperature, dosage, oil concentration in water and pH of the adsorbent were 15 to 75 mins, 20 to 100 °C, 0.3 to 1.5 g, 0.2 to 1.0 g/100 cm^3 and 2 to 10, respectively were selected. The coded and uncoded levels of these independent parameters are presented in Table 3.

2.10. Optimization modelling using machine language ANN

As an intelligent model, artificial neural network (ANN) is adept in simulating and modeling complex industrial processes (Babaei et al., 2016; Dil et al., 2016). It consists of various synchronous processing layers that are patterned after biological neurons. In this study, the layers include five input neurons that represent the five input parameters, unknown number of hidden neurons and one output neuron that denotes the percentage of oil removal. Hence, the ANN architecture is designated as 5-h-1 with h being the yet to be determined number of hidden neurons in the hidden layer as given in Fig. 1.

Table 2 Statistical Error analysis.

Error model	Equation	Equation number	Reference
Hybrid fractional error function	$HYBRID = \frac{100}{n-p}\sum_{i-1}^{n}\left[\frac{(q_{e,exp}-q_{e,cal})^2}{q_{e,exp}}\right]$	(13)	(Banerjee et al., 2006)
Average relative error	$ARE = \frac{100}{n}\sum_{i-1}^{n}\left[\frac{(q_{e,exp}-q_{e,cal})}{q_{e,exp}}\right]$	(14)	(Cheenmatchaya and Kungwakunakorn, 2014)
Marquardt's percent standard deviation	$MPSD = \frac{1}{n-P}\sum_{i-1}^{n}\left[\frac{(q_{e,exp}-q_{e,cal})^2}{q_{e,exp}}\right]$	(15)	(Cheenmatchaya and Kungwakunakorn, 2014)
Root mean square error	$RMSE = \frac{1}{n}\sum_{i-1}^{n}\left[\frac{(q_{e,exp}-q_{e,cal})^2}{q_{e,exp}}\right]$	(16)	(Paulauskiene et al., 2014)
Standard deviation	$SD = \frac{1}{n-1}\sum_{i-1}^{n}\left(\frac{q_{e,exp}-q_{e,cal}}{q_{e,exp}} - AARE\right)^2$	(17)	(Paulauskiene et al., 2014)
	$AARE = \frac{1}{n}\times\sum_{i-1}^{n}\left[\frac{(q_{e,exp}-q_{e,cal})}{q_{e,exp}}\right]$	(18)	(Nestor et al., 2004)

where $q_{e,exp} and q_{e,cal}$ are adsorption capacities obtained experimentally and adsorption capacities forecasted by the isotherm models, n is the number of experimental runs carried out whereas P is the number of isotherm parameters or factors. In addition to the correlation coefficient, the error analysis was also used to verify the key models RSM, ANN and ANFIS. They were used to rank the models based on higher correlation coefficient and lower SSE, ARE, RMSE, HYBRID and MPSD terms.

Table 3 Uncoded and coded levels of independent variables for crude oil removal by BPF.

Variable	Symbol	Axial (-α)	Low	Center	High	Axial (+α)
Level		−2	−1	0	1	2
Temperature (°C)	X_1	0.0	20	60	100	140
Oil Concentration (g/100 cm^3)	X_2	0.0	0.2	0.6	1.0	1.4
Adsorbent dosage (g)	X_3	0.0	0.3	0.9	1.5	2.1
pH	X_4	0.0	2	6	10	14
Time (mins)	X_5	0.0	15	45	75	105

The data sets used in RSM was quintupled and used in the neural network modeling since the performance and reliability of the ANN is enhanced with lager number of data sets (Asadu et al., 2022). Marquadt Levenberg (ML) algorithm was used in the training the ANN data with error minimization achieved with gradient descent while training function was used to regularize the bias value (Meybodi et al., 2015; Karimi et al., 2012). Before the overall modeling, the data sets were first divided into training, testing, and validation with 60%, 20%, and 20% of the total data sets respectively. The network training provides an empirical relationship between the output and input factors. The network testing measures the predictability of the ANN model while the network validation ensures generalization of the neural model. The process parameters were normalized so as to minimize network error (Mourabet et al., 2014).

2.11. Optimization modelling using machine language ANFIS

ANFIS is hybrid model of neural and fuzzy networks that can model complex nonlinear process with speed and accuracy (Bahman and Sina, 2018). In this study, Sugeno inference system which converts input parameters into membership values though membership functions (MF) were used. It is a five-layered model with the layers representing input, input-mf, rule, output-mf and output respectively. The input layer represented the five input factors (temperature, oil concentration, adsorbent dosage, pH, and contact time) while the output layer represented the percentage of oil removal as shown in Fig. 2. In generating the fuzzy inference system (FIS), three MFs were assigned to each input factor. The same number of ANN data sets was used in the ANFIS modeling. The data set was equally fragmented into training, testing, and checking/validation with 60%, 20% and 20% representing approximately 80, 26, and 26 data sets respectively.

3. Results and discussion

3.1. The proximate analysis results

The results of characterization of the raw, carbonized and esterified BPF were presented in Table 4. Untreated or raw BPF consist mainly of cellulose (36.3%), lignin (18.5%), volatile matter (41.6%), fixed carbon (29.4%) and surface area (295.6 cm^2) as could be seen in Table 4. Increased percentage carbon noticed in the untreated BPF displays its prospects as sorbent. Biomass with sufficiently high percentage carbon has adsorptive prospects as presented by Ogbodo et al., 2021; Fazal and Rafique, 2013. Volatile matter reduced after thermal treatment showing the influence of carbonization (20.1%) and equally reduce more to (10.3%) after impregnation with acid for esterification reaction. Also, fixed carbon grew from 29.4% to 69.1%. This process agreed favorably with the report by Omar, 2012, which describe how thermal treatment eliminates volatile components of biomass leading to increased fixed carbon and number of pores within the surface. Moreover, esterification expanded the surface area from 295 cm^2/g to 556.8 cm^2/g in agreement with earlier report on

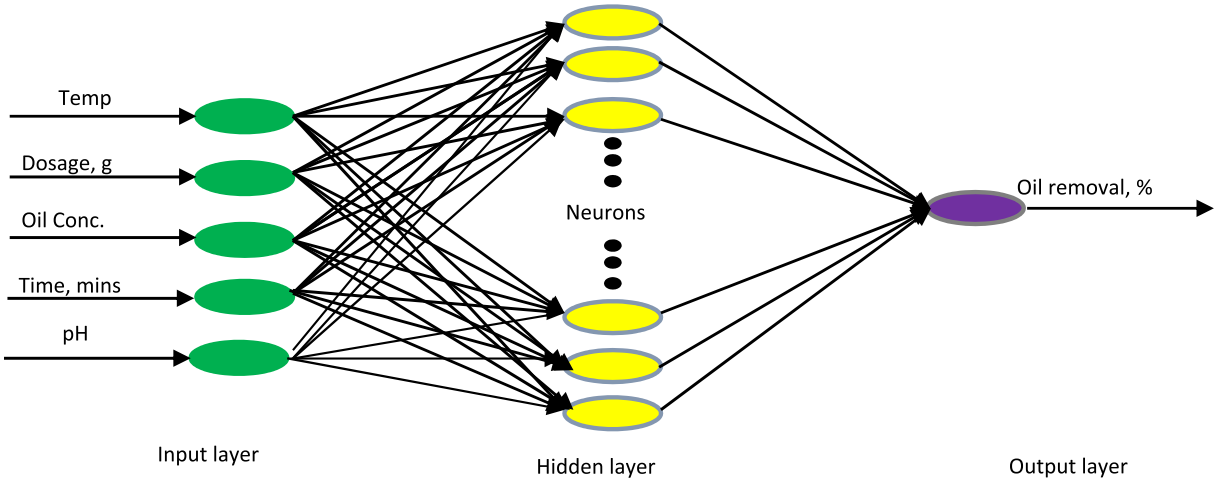

Fig. 1 ANN architecture of the oil removal process.

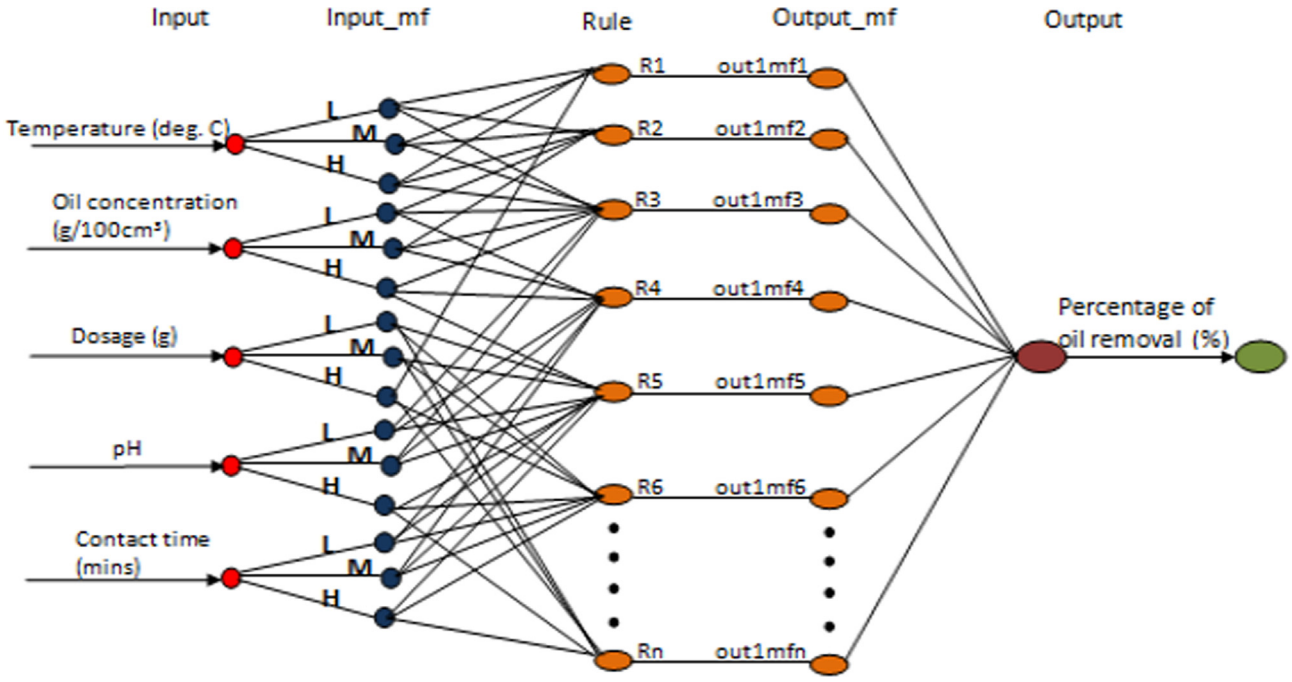

Fig. 2 The ANFIS architecture showing the five layers.

Table 4 The proximate composition of treated and untreated BPF.

Properties	BPF		
	Raw	carbonized	Esterified
Fixed carbon (%)	29.4	58.5	69.1
Volatile matter (%)	41.6	20.1	10.3
Ash Content (%)	10.0	9.7	11.4
Surface area (cm^2/g)	295.6	302.1	556.8
Moisture content (%)	19.14	11.06	9.2
Lignin (%)	18.5	17.2	15.6
Cellulose (%)	36.3	35.8	34.9

the adsorptive prospect of the modified BPF. This result is quite higher than the surface area of 374.3 cm^2/g and 275.4 cm^2 presented by Akpomie and Conradie, 2020 and Ahmad and Danish, 2018, respectively after Alkaline activation of other agro wastes. The high percentage of lignin and cellulose explained the reason for the high tensile strength of the adsorbent to keep the islands and pores within the surface after heating activities.

3.2. SEM analysis of untreated and treated BPF

Fig. 3a shows the SEM image of the untreated BPF at various magnifications. A weight of micro-structure with homogenous connections of materials having minimal filamentous and fistu-

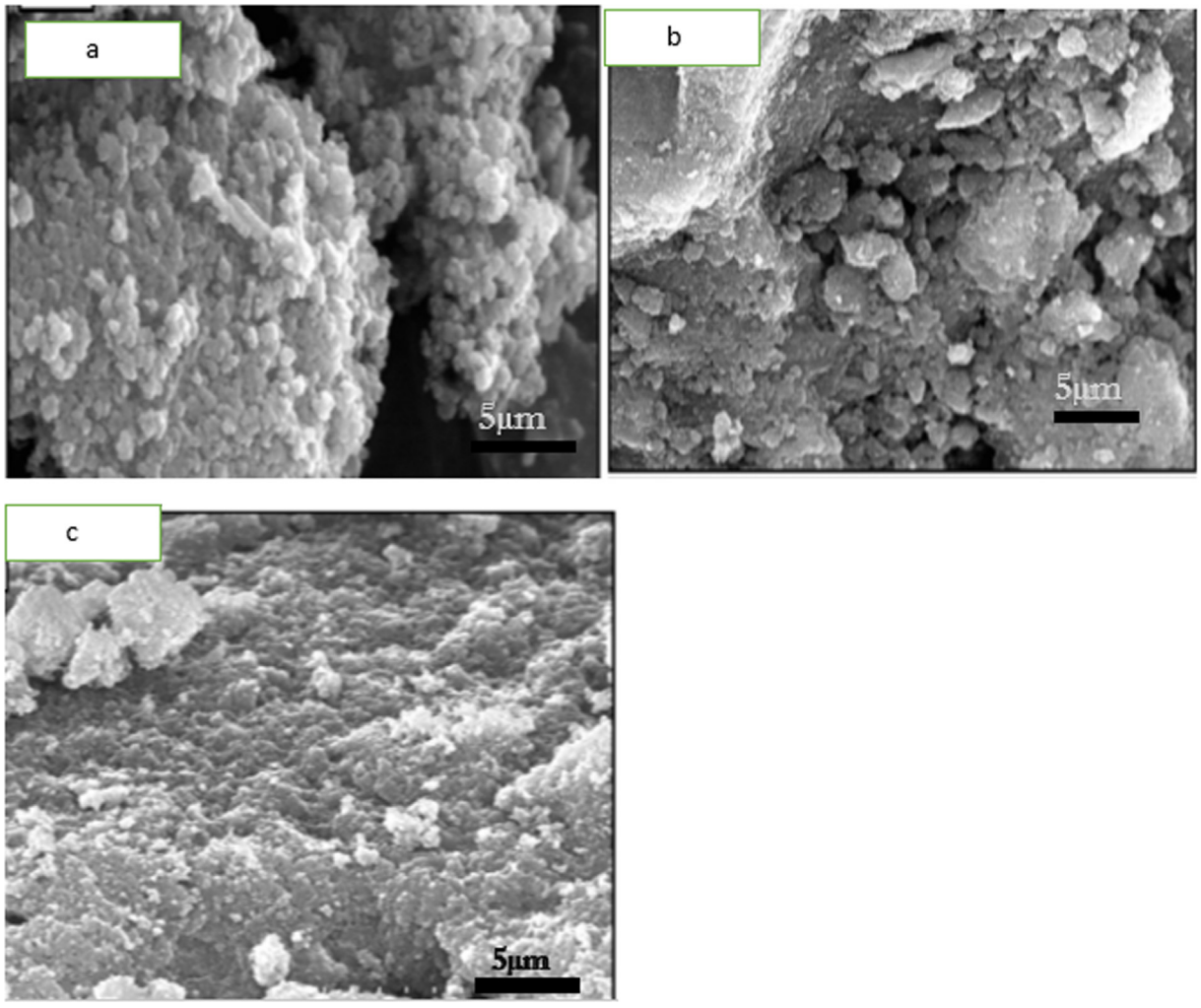

Fig. 3 SEM image of (a) Uncarbonized or raw BPF (b) Carbonized BPF and (c) Esterified BPF.

lous crystallites confirming the presence of minerals is shown in Fig. 3a. The surface is made up of primarily a lignocellulosic network and interfibrillar matrix that have lignin, cellullose volatile organic compounds and hemicellulose. This generates microporous structure in the surfaces displaying the porosity of the BPF which aids in the crude oil removal.

Fig. 3b and 3c are the SEM images of treated BPF, which shows various cumulative particles. The porosities of the treated BPF (Fig. 3b and 3c) are higher than that of the untreated BPF (Fig. 3a) giving strong proof that great number of solid particles (inorganic parts or most volatile parts) were removed through heat treatment or acid treatment. It can also be seen that the porosity of the organic acid treated BPF showed in Fig. 3c has more void spaces compared with both untreated and carbonized BPF depicted in Fig. 3a and 3b. The carbonized BPF seems to have less void spaces showing that treatment with stearic acid increased the porosity of the BPF by producing more numbers of pores within the surface. These can be alluded to the reaction of the acid with inorganic solid particles in the pores leading to more void volumes.

3.3. FT-IR of untreated and treated BPF

Presented in Table 5 are the spectrums of untreated and esterified BPF, with bands within 3900, 2900, 1738, 1646, 1254, 1072 and 895 cm^{-1} carefully and tactically defined. The peaks show lignocellulosic substances with extended bands of hydroxyl group (OH) and intermolecular hydrogen at the desired frequencies around 3210–3351 cm^{-1}. A polysaccharide semi crystalline solid which may be cellulose having bonds with a number of OH was discovered. Around 3451 cm^{-1}, the broad bands could likely be as a result of C—H vibration stretching of cellulose and hemicellulose. Between 3322 and 2921 cm^{-1}, the bands appear to be as a result of the presence of cellulose showing that the remaining bands are lignin. Some bands with aromatic rings in nature were noticed, and they might be due to presence of lignin. The aromatic bands manifesting as C=C were observed around 1451, 1511, 1591 and as well at 1611 cm^{-1}. New ester bonds and hydroxyl group were introduced to the cellulose with the elimination of some inorganic substances that was shown by the peaks that are more ener-

Table 5 FTIR spectrum with assigned functional groups for raw and treated BPF.

Raw BPF Frequency (cm^{-1})	Carbonized BPF Frequency (cm^{-1})	Assigned functional group	Esterified BPF Frequency (cm^{-1})
3621.6	3731.4	O—H stretch	3701.8–3982.5
–	3585.2	Hydroxyl group, H-bonded, O—H stretch	–
3458.4	3233.9	NH stretch	3321,3
–	–	Aliphatic secondary amine, NH stretch	3250.3
3049	3091.1	Normal "polymeric" OH stretch	2913.8
27,401	–	Methylamino, N—CH_3, C—H stretch	–
2288.6	2245.6	Isocyanate (—N═C═O asym. Stretch)	–
2074.3–2126.7	2153.4–2186.1	Cyanide ion, thiocyanate ion and related ions	2089.5
1915.7–1974.3	1858.1	Aromatic combination	1980.3
1706.3–1800.4	–	Isothiocyanate (—NCS)	–
1597.7–1687.7	1640.6–1821.3	Conjugated ketone, open-chain acid anhydride	1674.3
1513.3–1576.7	1580.4	C═C—C Aromatic ring stretch	1552.7
14228.7	–	O—H bend	1431.6
1304.2	1364.2	N—O asymmetric stretch	13203.1
1103.3	1125.8	Aromatic C—H in plane bend	–
1047.4	1067.259	Aromatic C—H in plane bend,	1063.6
873	–	Peroxides, C—O—O— stretch	–
–	783.6	C—Cl stretch, Alkyne C—H bend	778.3
	–	C—Cl stretch, Alkyne C—H bend	684.2

getic around 1745 cm^{-1} stretching at —C═O and 1243 cm^{-1} stretching at C—O at end of esterification reaction between BPF and stearic acid. The effect of heat treatment and acid treatment is clearly seen in Table 5 since most of the functional group appear to be missing out while some persisted. The removal of these functional groups are due to thermal treatment and the reaction of acid with some inorganic compounds.

3.4. Effect of process parameters on crude oil adsorption by BPF

3.4.1. Effect of pH

Fig. 4a depicts the effect of pH on the BPF biomass removal of oil layer. It was noticed that ideal or optimum removal of oil using esterified BPF was 96.8% at pH of 4. Interestedly, the oil removal rate reduced significantly with increase in pH. This is in good agreement with the report of Bansal et al., 2011; Dil et al., 2019b which stated that oil is insoluble in water because it contains bonds that repels particles with similar electro negativities and net dipole. The reduction in oil removal rate with increase in pH confirm the results from pH charge study which revealed that the outer layers of the BPF mainly consist of positive ions. This could be that as pH is reduced, the level of the biomass (BPF) outer layer protonation seems to be more, leading to more spreading onto the void volume or space. Thus, the inclination toward crude oil removal due to attractive force between the positive surface and negatively charged oil layers. This idea agreed with works by other researchers in literature (Awual et al., 2016; Naema et al., 2014; Pragnesh et al., 2011). Esterified BPF performed better as clearly shown in Fig. 4a, this could be because of more pore formation on the outer layer of BPF due to the reaction between stearic acid with inorganic parts of the biomass.

3.4.2. Effect of temperature

The dependency of Crude oil removal on temperature were estimated using the produced BPF as shown in Fig. 4b. It can be seen from Fig. 4b that crude oil removal by the BPF adsorbents is sensitive to temperature. The optimum temperature for oil removal was obtained as 80 °C since there was no change in oil removal rate above 80 °C. Increase in oil removal rate with increase in temperature may be because rising temperature increases the rate of diffusion or dispersion of oil molecules across the boundary layer and inside pores of the BPF particles. Esterified BPF achieved the highest oil removal rate of 95.3% at temperature of 80 °C thereby supporting the earlier result by Behnood et al., 2013 that biomass treated with organic acid has higher prospect for crude oil removal. The carbonized BPF had 82.4% whereas the untreated BPF had as low as 61.8% at the temperature of 80 °C. Comparative pattern was something similar for the three adsorbents yet esterified BPF at a similar temperature and time recorded the most elevated rate of oil removal. Temperature affects the rate of oil removal by altering the interaction of oil molecules and the dissolvability of the oil. The increase in adsorption of oil layers with increase in temperature will enhance the movability of the oil particles and produce greater result inside the adsorbent. Similar work by different researchers in the literature emphasized similar pattern (Rashmi and Bhattacharya, 2003; Verma and Mishra, 2010; Ahmadi et al., 2016).

3.4.3. Effect of oil water ratio

Fig. 4c shows the effect of oil removal from water surface via BPF was studied using oil–water ratio ranging from 0.2 to 1.0 g/100 cm^3. It is obvious from Fig. 4c that increment of amount of oil on water outer layer without comparative addition in adsorbent dose of BPF reduced the BPF adsorbent rate of oil removal. This might be because porous surfaces of BPF that are accessible for oil removal were increasingly saturated as the crude oil spreads on the surface. The sorption of oil by the esterified and untreated BPF followed the same manner, but esterified BPF achieved the highest removal rate of 98.2% at initial oil–water concentration of 0.2 g of oil in 100$cm^3$of water. The amount of oil removed per unit mass increased with an increase in initial concentration of oil, the adsorption rate reduced. This can be explained by the fact that the amount of significant number of the oil particles to accessible surface area at lower concentration is low (Arivoli et al., 2019; Moghaddam et al., 2019; Berizi et al., 2016).

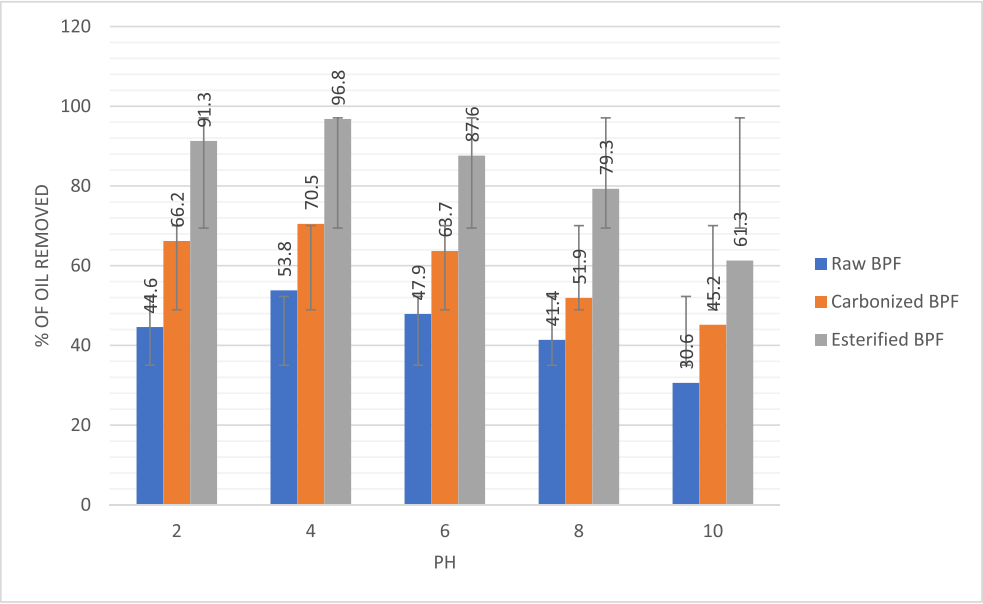

Fig. 4a Effect of pH on crude oil removal by the BPF adsorbents.

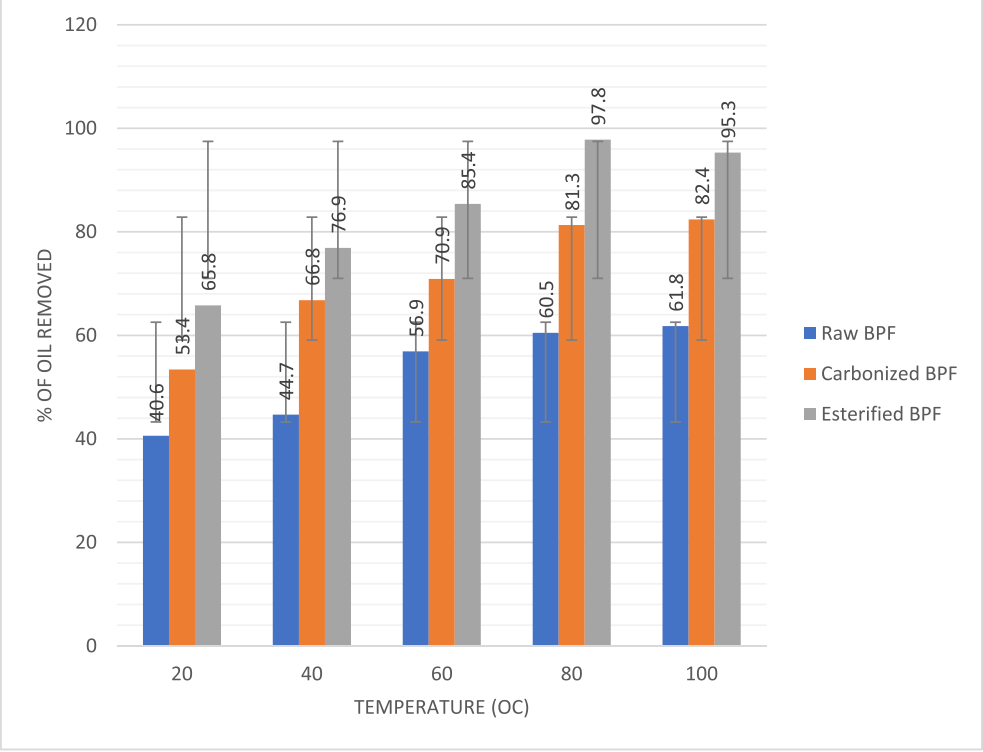

Fig. 4b Effect of temperature on crude oil removal by BPF adsorbent.

3.5. Thermodynamic modeling of the adsorption process

The activation energy values acquired from the slope of the plot of In K against 1/T (K^{-1}) in equation (9) for the first order model is shown in Table 6. The activation energy for the diffusion of molecules onto BPF is 18.56 kJ/mol, which was lower than those reported in literature by Thompson et al., 2020, (44.29 kJ/mol) for the diffusion of lead ion onto cassava peels adsorbent using first order process. Though, the activation energy procured using BPF is within the range reported by Naema et al., 2014 for lead adsorption onto Petiol and Fiber palm tree adsorbents.

Similarly, activation energy obtained from the slope of the plot of In K against 1/T (K^{-1}) in equation (9), for the second

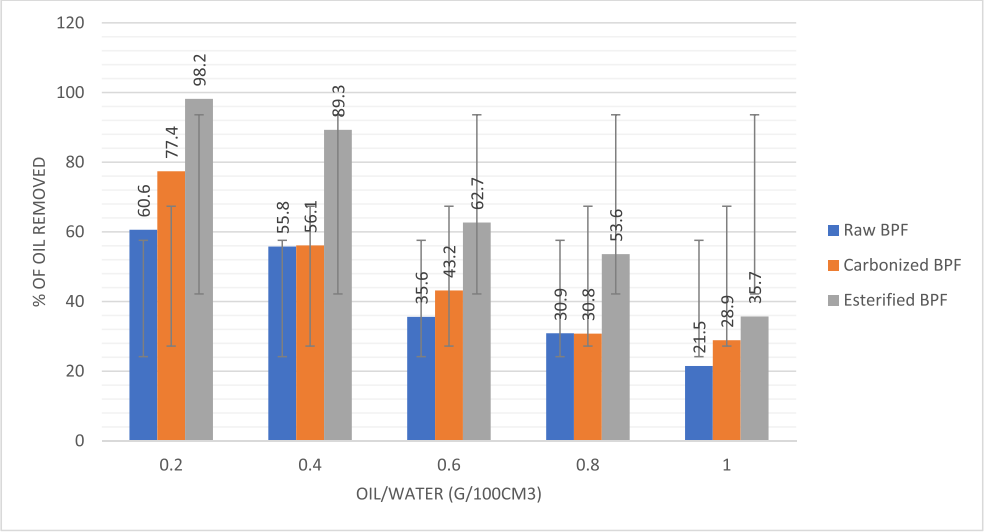

Fig. 4c Effect of oil water ratio on crude oil removal by BPF adsorbent.

Table 6 Thermodynamics parameters of crude oil sorption by BPF for first and second order models.

	Irreversible pseudo-first order model				Irreversible pseudo-second order model			
T (K)	E_a kJ/mol	ΔH kJ/mol	ΔS kJ/mol	ΔG kJ/mol	E_a kJ/mol	ΔH kJ/mol	ΔS kJ/mol	ΔG kJ/mol
318				16.23				51.47
323				18.17				52.44
328	18.56	25.44	−0.751	21.37	25.77	29.16	−0.813	55.17
333				27.24				58.12
338				30.15				58.83

order model is equally presented in Table 6. The activation energy for BPF sample diffusion is 25.77 kJ/mol, which is within the range of 38.33 kJ/mol reported by Chinonye et al., 2018 for the second order adsorption of orange G onto kola nut shell. It could be observed that the Ea value for second order kinetic is higher than that of the first order model, which could be ascribed to the higher rate constant value of the pseudo-second order model compared with the pseudo-first order model. Also, Behnood et al., 2016 reported similar result in their work.

The Eyring plot (see equation (10)) for the sorption and diffusion of oil molecules for irreversible pseudo first and second order models were displayed. The values of the thermodynamic parameters (ΔH, ΔS and ΔG) obtained from the plots of 1/T vs Ln (k/T) using equation (10) for the pseudo-first order model were displayed in Table 6. Also, the values of thermodynamic parameters (ΔH, ΔS and ΔG) for the pseudo-second order model using equation (10) were shown in Table 6.

The enthalpy change, ΔH for the irreversible pseudo first order model for adsorption of oil onto esterified BPF is 25.44 kJ mol^{-1} as shown in Table 6. The positive value shows that energy is absorbed from external source in order to raise the energy level for easier oil molecules diffusion to the transition state. This shows that the process is endothermic (Asadu et al., 2021a,b; Asadu et al., 2019. This enthalpy value is comparable in range to the 16.35 kJ mol^{-1} obtained for oil sorption by spent camellia sinnensis biomass reported by Falaz and fafique, 2013. For the entropy change, the value for the irreversible pseudo first order transesterification of BPF is −0.751 kJ/mol (see Table 6), the negative value shows the degree of existing associative mechanism where diffusion species joined together to produce more ordered transition state (Verma and Mishra, 2010). The value falls within the range reported by Awual et al., 2013 (−0.121 kJ mol^{-1} K^{-1}) and Onwu et al., 2019b, (−0.18 kJ mol^{-1} K^{-1}), for the sorption of waste cooking and soybean oils respectively.The change in Gibb's free energy ΔG value for the irreversible pseudo first order sorption of oil by BPSF were in the range of 16.23–30. 15 kJ mol^{-1} as shown in see Table 6. The positive value of ΔG shows the non-spontaneous form of the process (Nwabanne et al., 2018), but the value is lower than 88.23 kJ mol^{-1} and 83.30–87.69 kJ mol^{-1}, presented by Ladhe et al., 2011 and Thompson et al., 2020, for the sorption of waste cooking oil and lead ion respectively.

The enthalpy, ΔH value of the irreversible pseudo second order model for adsorption of crude oil onto BPF is 29.16 kJ mol^{-1} as presented in Table 6. Also the positive ΔH reveals that external energy input (heat) is needed to lift the energy level for change of reactants to their transition state. Thus, the process is endothermic (Albert et al., 2016). This enthalpy, ΔH value of the irreversible pseudo second order

for adsorption of crude oil onto BPF is within the range (28.33 kJ mol^{-1}) reported by Abert et al., 2016 for the soybean waste adsorbent.

The entropy change, ΔS for the irreversible pseudo second order for crude oil adsorption onto BPF is − 0.813 kJ mol^{-1} K^{-1} as presented in Table 6. As explained earlier, negative value of ΔS shows an existence of associative mechanism where reactants joined together to produce more arranged transition state (Thompson et al., 2020). As in the first order, the value acquired fell within the range (−0.121 kJ mol^{-1} K^{-1}) presented by Awual et al., 2016 for palm oil adsorption from water.

Finally, the value of free energy change, ΔG for the irreversible pseudo second order for crude oil sorption by BPF also fell within the range of 51.47–58.83 kJ mol^{-1} as shown in Table 6, with positive values showing the non-spontaneous form of the adsorption process (Egbuna et al., 2019a). The value was comparable to 88.23 kJ mol^{-1} presented by Onwu et al., 2019b for crude oil sorption onto groundnut shell.

3.6. Equilibrium modelling of oil sorption onto BPF

According to report by Asadu et al., 2018, adsorption isotherm is a significant requirement for planning any sorption structure. It is the relationship between the amount of substance removed from fluid stage per unit mass of acid treated biomass adsorbent and its value at constant temperature (Sheela Tand Arthoba, 2012; Rahman and Haseen, 2014). Effectiveness of the models (see Table 1) was utilized and examined. The isotherm border and correlation coefficient (R^2) evaluated from the plots of the straight fittings were introduced (see Table 7). R^2 was used to simulate the model with the best fit. The evaluated dimensionless quantity for Langmuir model known as separation factor (R_L) at the four assigned temperatures were <1(0.1067, 0.2056, 0.3501 and 0.3301) indicating ideal sorption. This insight can be due to the uniform or homogeneity of dynamic distribution of active site on the outer surface of the esterified BPF (Asadu et al., 2021b). K_f (in Freundlich isotherm model as shown in Table 1) as a constant is a proportion of the adsorption limit while *n* is a proportion constant of the intensity of the sorption process (Sheela Tand Arthoba, 2012; Rahman and Haseen, 2014). For beneficial adsorption, the value of *n* lies within the range of 1–10 (Nwabanne et al., 2018; Awual et al., 2013). From Table 7, it can be clearly seen that the value of *n* at four specific temperatures were within the range of 1–10 (1.3845,2.8359, 3.3401 and 3.8940) revealing a helpful sorption for oil layer onto esterified BPF. K_f for equation 6 increased with increase in temperature as presented in Table 7, showing that the extent of adsorption of oil onto esterified BPF relied on high temperature. Equation (11) shows that if the energy needed for activation (E) is below 8 kJ/mol, the interaction is physisorption, but if the activation energy lie between 8 kJ/mol and 16 kJ/mol, the cycle is chemisorption in nature (Kudaybergenov et al., 2015). In addition, the mean free energy of sorption per mole of the adsorbate (Bd) shows that adsorption is restricted by particle diffusion mechanism and $E > 16$ kJ/mol implies an adsorption is represented by molecule dispersion system (Onu et al., 2021, 2022). It is obvious from Table 7 that the activation energy was below 8 kJ/mol at each temperature under investigation showing that the introduction of unrefined oil from water surface by the esterified BPF is physisorption. Besides, the qualities for Bd at the chosen temperatures examined were below 16 kJ/mol suggesting that the sorption of crude oil onto BPF might not have been controlled by particle diffusion mechanism. The R^2 at each temperature studied suggested that the sorption of oil onto esterified BPF might have dependency on Langmuir iso-

Table 7 Isotherm parameters evaluated for oil removal by esterified BPF.

Model	Temperature (K)			
	303	323	343	363
Langmuir				
q (mg/g)	25.345	26.168	27.089	23.547
K_L (L/mg)	0.348	2.0123	1.8801	1.9458
R_L	0.1067	0.2056	0.3501	0.3301
R^2	0.991	0.997	0.996	0.998
Dubinin Radushkevich				
B_d	0.0103	0.00183	0.02301	0.0320
q_m (mg/g)	23.871	87.012	77.013	56.879
R^2	0.823	0.903	0.913	0.928
E (kJ/mol)	2.387	2.0083	1.134	1.0569
Freundlich				
n	1.3845	2.8359	3.3401	3.8940
K_f(L/g)	30.012	28.292	32.903	34.147
R^2	0.916	0.908	0.938	0.920
Temkin				
b (J/mol)	11.44	13.78	23.56	36.44
K_T (L/g)	2.300	3.561	4.089	5.236
R^2	0.823	0.946	0.935	0.941
Elovich				
q_m(mg/g)	37.321	28.375	36.018	40.182
Ke	2.234	1.7841	3.478	2.214
R^2	0.941	0.905	0.935	0.921

Table 8 Calculated parameters and statistical error analysis on the isotherm models for the sorption oil onto esterified BPF.

Isotherm model	R^2	q_{exp}	q_{cal}	SD (%)	HYBRID (%)	MPSD (%)	RMSE (%)	ARE (%)
Langmuir $\frac{C_e}{q_e} = \frac{1}{q_m K_e} + \frac{C_e}{q_m}$	0.998	49.33	51.23	6.08	12.34	7.82	4.51	10.11
Freundlich $Logq_e = LogK_f + \frac{1}{n} LogC_e$	0.928	49.33	54.38	13.11	18.68	12.86	20.22	17.93
Dubinin- Radushkevich $Inq_e = Inq_m - \beta E^2$	0.920	49.33	55.71	31.6	27.10	38.6	21.41	26.56
Temkin $q_e = \frac{Rt}{b} InK_T + \frac{Rt}{b} InC_e$	0.941	49.33	56.09	19.9	22.15	17.89	13.38	18.12
Elovich $In\frac{q_e}{C_e} = InK_e q_m - \frac{q_e}{q_m}$	0.921	49.33	48.15	20.7	24.32	10.04	16.31	14.08

therm model since the R^2 are approximately 1 compared with other models at each temperature under study as shown in Table 7.

3.7. Isotherm model performance index

Validation of the performance of the equations listed in Table 1 was successfully carried out using statistical tools like standard deviation (SD), hybrid fractional error function (HYBRID), average relative error (ARE), Marquardt's percent standard deviation (MPSD), and root mean square error (RMSE). Predicted adsorption capacity (q_{cal}) and experimental adsorption capacity (q_{exp}) were utilized. The outcomes of the analysis were outlined in Table 8. The smaller the values of SD, HYBRID, MPSD, RMSE and ARE the more corresponding the set of data and better the goodness of fit (Ladhe et al., 2011). It is clearly seen in Table 8 that the data on the sorption of crude oil onto esterified banana peels fiber adsorbent sufficiently fits onto Langmuir isotherm model since it seems to have the smallest values for every used statistical tools SD (6.08%), HYBRID (12.34%), MPSD (7.82%), RMSE (4.51%) and ARE (10.11%) confirming and given credence to the earlier prediction by correlation coefficient (R^2) and separation factor (R_L) in Table 7.

3.8. ANOVA analysis and model fitting of RSM data

The ranges and the levels of the independent parameters examined for the adsorption process via Minitab 17.0 software were shown in Table 3. The percentage adsorption by esterified BPF at various experimental situations according to the design matrix were presented in Table 9. The evaluation of the effects of the independent parameters on the dependent variable (% of oil removed) was performed using multiple regression analysis (Rahman et al., 2021a; Bagheri et al., 2019). The percentage of oil removed obtained from experiments was analyzed using many experimental approaches of regression, in order to fit the 2nd order polynomial model expression.

The importance of the model equation and terms were assessed using ANOVA test (see Table 10). The regression coefficient of the intercept and the linear and quadratic as well as the interaction terms of the model for percentage oil adsorbed utilized for the adsorption examined were shown in Table 11. Also, estimated F_{value} > the F_{table} or critical F_{value} is a pointer that the model sufficiently fitted the experimental data (Egbuna et al., 2019a; Ugwele et al., 2020). From Table 10, on 95% confidence level, the model was considered to be sufficient, since estimated F_{value} (27.48) was more than the tabulated $F_{0.05,10,10}$ value (2.06). In addition, the model terms were also confirmed for significance at 95% confidence level. The tabulated $F_{0.05,1,10}$ value was 4.23. Thus, the listed terms in the model, $(X_1, X_2, X_3, X_4, X_5, X_1^2, X_2^2, X_3^2, X_4^2, X_5^2, X_1X_3, X_2X_4, X_3X_4)$ were all significant.

It is consequential at this point to state that the p-value was utilized to discover if a statistical premise is important or not and how important it is. On the foundation of 95% confidence level, when the determined p-value is < critical p = 0.05, there is stronger proof against null hypothesis or the theory H_0 (Chinonye et al., 2018; Asadu et al., 2019; Onu et al., 2021, 2022). Therefore, the model for percentage of oil adsorbed by BPF was discovered be important because its p-value was = 0.000 and < 0.05 (see Table 8). Also, from Table 10, the listed terms $(X_1, X_2, X_3, X_4, X_5, X_1^2, X_2^2, X_3^2, X_4^2, X_5^2, X_1X_3, X_2X_4, X_3X_4)$ were all significant at ($p < 0.05$) for oil sorption by BPF.

The entire regression equation, model terms and the statistical significance were evaluated using Minitab 17.0 software. For the adsorption of oil by BPF, the second-order polynomial regression model that explained the process (% of oil removed) best as a function of actual values of temperature (X_1), oil concentration (X_2) and dosage (X_3), pH (X_4) and time (X_5) (see equation (13)).

$$\begin{aligned}[\%\ Removed]_{BPF} = {} & 87.02 + 2.74X_1 + 3.76X_2 + 3.22X_3 \\ & + 2.87X_4 + 6.20X_5 - 01.03X_1^2 \\ & - 2.74X_2^2 - 1.48X_3^2 - 1.63X_4^2 \\ & - 1.68X_5^2 - 0.73X_1X_2 - 1.01X_1X_3 \\ & - 0.23X_1X_4 + 0.17X_1X_5 \\ & - 0.63X_2X_3 - 0.92X_2X_4 \\ & + 0.59X_2X_5 - 1.12X_3X_4 \\ & + 0.83X_3X_5 - 0.01X_4X_5 \end{aligned} \quad (13)$$

Table 9 Design matrix of coded variables with responses for oil removal by BPF.

Standard run	Run order	Coded value	Temp (°C) ;X_1	Oil/water (g/100 cm^3) :X_2	Sorbent dosage(g) :X_3	pH :X_4	Time (min) :X_5	% Of oil Removed	
								Experiment	RSM
30	1	−1	60	0.6	0.9	14	45	92.20	92.462
25	2	−1	60	−0.2	0.9	6	45	83.31	83.219
29	3	−1	60	0.6	0.9	−2	45	90.50	90.226
24	4	−1	140	0.6	0.9	6	45	88.55	88.627
31	5	−1	60	0.6	0.9	6	−15	71.89	71.801
26	6	−1	60	1.4	0.9	6	45	91.46	91.539
33	7	0	60	0.6	0.9	6	45	87.93	87.990
23	8	−1	−20	0.6	0.9	6	45	93.02	92.931
28	9	−1	60	0.6	2.1	6	45	84.62	84.507
27	10	−1	60	0.6	−0.3	6	45	81.32	81.421
32	11	−1	60	0.6	0.9	6	105	82.53	82.607
5	12	1	20	0.2	1.5	2	15	88.50	88.660
19	13	0	60	0.6	0.9	6	45	90.65	90.615
14	14	1	100	0.2	1.5	10	15	82.26	82.244
3	15	1	20	1.0	0.3	2	15	90.92	90.984
11	16	1	20	1.0	0.3	10	75	90.83	90.718
8	17	1	100	1.0	1.5	2	15	87.51	87.585
7	18	1	20	1.0	1.5	2	75	92.74	92.815
22	19	0	60	0.6	0.9	6	45	90.65	90.615
1	20	1	20	0.2	0.3	2	75	83.90	83.965
12	21	1	100	1.0	0.3	10	15	85.68	85.568
6	22	1	100	0.2	1.5	2	75	90.91	90.986
9	23	1	20	0.2	0.3	10	15	88.89	88.862
17	24	0	60	0.6	0.9	6	45	90.55	90.615
10	25	1	100	0.2	0.3	10	75	93.31	93.199
4	26	1	100	0.2	1.5	2	75	94.07	94.050
18	27	0	60	0.6	0.9	6	45	90.60	90.615
13	28	1	20	1.0	0.3	10	75	88.98	88.964
15	29	1	20	1.0	1.5	10	15	88.02	88.003
20	30	0	60	0.6	0.9	6	45	90.65	90.615
16	31	1	100	1.0	1.5	10	75	91.38	91.280
2	32	1	100	0.2	0.3	2	15	70.78	70.845
21	33	0	60	0.6	0.9	6	45	90.64	90.615

Similarly, equation (14) shows the model expression for the % of oil adsorbed or removed after all inconsequential terms were removed. The removal of these inconsequential terms were neccessitated by their p-values (see ANOVA), that were > 0.05 (see Table 10).

$$[\%\ Removed]_{BPF} = 87.02 + 2.74X_1 + 3.76X_2 + 3.22X_3 + 2.87X_4 + 6.20X_5 - 01.03X_1^2 - 2.74X_2^2 - 1.48X_3^2 - 1.63X_4^2 - 1.68X_5^2 - 1.01X_1X_3 - 0.92X_2X_4 - 1.12X_3X_4 \quad (14)$$

The regression coefficient (R^2) and the adjusted R^2 are the variables of interest that were utilized to present the goodness of fit of the suggested second order polynomial model (see Eq. (14)). As could be seen in Table 11, the R^2 value for % oil adsorption is 99.97. Hence, the closer the value of R^2 to 1 (100%), the better the selected model in predicting the response (Onyekwelu et al., 2021; Ezedinma et al., 2021). Similarly, the Adj-R^2 value for crude oil adsorption by BPF is 99.90. The R^2 value shows noteworthy approximation to 1, hence, an indication of efficient fit. As evident in Table 11, the values of the predicted models R^2 and Adj-R^2 were both found to be very high. Therefore, the closeness between R^2 and Adj-R^2 values, in addition to the lower value of Adj-R^2 compared to that of R^2, for all the model, is an indication of goodness of the data fit.

3.8.1. Dosage-pH interaction effect

The response surface plot and contour plots for the impact of pH and temperature interactions (X_3X_4) on the percentage sorption of oil by the activated biomass are depicted in Fig. 5. The interaction of dosage and pH for the crude oil removal using esterified BPF was significant at $p < 0.05$ as shown in Table 10. It can be seen that the contour was curve which is an indication of good interaction. The 3D curve slope backward indicating that high dosage and low pH yielded high percentage removal.

3.8.2. Temperature - dosage interaction effect

Fig. 6 depicts the response surface plots and contour plots for the impact of temperature – dosage interactions (X_1X_3). The interaction of temperature and dosage was significant at $p < 0.05$ as presented in Table 10 for the crude oil adsorption

Table 10 ANOVA for response surface quadratic model of the process of oil sorption by esterified BPF.

Source of Variable	SS	Df	Coeff. (β)	SE coeff.	MS	F-value	P-value	T-value
Model (C)	3649.02	21	89.582	0.981	173.76	27.48	0.000	91.35
Blocks	77.42	1	0.000	0.964	77.42	11.35	0.006	0.00
X_1	301.68	1	3.545	0.533	301.68	44.24	0.000	6.65
X_2	398.13	1	4.073	0.533	398.13	58.39	0.000	7.64
X_3	352.90	1	3.835	0.533	352.90	51.76	0.000	7.19
X_4	126.36	1	2.295	0.533	126.36	18.53	0.001	4.30
X_5	1375.77	1	7.571	0.533	1375.77	201.77	0.000	14.20
X_1^2	58.29	1	−1.835	0.475	101.73	14.92	0.003	−3.86
X_4^3	169.00	1	−2.696	0.475	219.65	32.21	0.000	−5.68
X_4^2	103.29	1	−2.092	0.475	132.29	19.40	0.001	−4.40
X_5^2	148.54	1	−2.346	0.475	166.32	24.39	0.000	−4.94
	171.68	1	−2.383	0.475	171.68	25.18	0.000	−5.02
X_1X_2	1.20	1	−0.274	0.653	1.20	0.18	0.682	−0.42
X_1X_3	5.44	1	−0.583	0.653	5.44	0.80	0.031	−0.89
X_1X_4	50.30	1	1.773	0.653	50.30	7.38	0.020	2.72
X_1X_5	22.54	1	−1.187	0.653	22.54	3.31	0.096	−1.82
X_2X_3	170.11	1	−3.261	0.653	170.11	24.95	0.000	−4.99
X_2X_4	42.48	1	−1.629	0.653	42.48	6.23	0.030	−2.50
X_2X_5	2.04	1	−0.357	0.653	2.04	0.30	0.596	−0.55
X_3X_4	52.02	1	−1.803	0.653	52.02	7.63	0.018	−2.76
X_3X_5	0.28	1	−0.133	0.653	0.28	0.04	0.842	−0.20
X_4X_5	19.56	1	1.106	0.653	19.56	2.87	0.118	1.69

[C] Constant.
[SS] stands for Sum of squares.
[Df] stands for Degree of freedom.
[Coeff.] stands for Coefficients.
[SE Coeff.] stands for SE Coefficient.
[MS] stands for Mean square.
X_1: temperature; X_2: oil concentration; X_3: dosage of BPSF; X_4: pH; X_5: time.
$p < 0.01$ highly significant; $0.01 < p < 0.05$ significant; $p > 0.05$ not significant.
Model Tabulated $F_{0.05,10,10}$ value is 2.06. Hence, $F > 2.06$ significant; $F < 2.06$ insignificant.
Model terms Tabulated $F_{0.05,1,10}$ value is 4.23. Hence, $F > 4.23$ significant; $F < 4.23$ insignificant.

Table 11 Analysis of variance of regression for response surface model of the % of oil adsorbed on the BPF sample.

Regression	R^2 (%)	Adj. R^2 (%)	F-value	P-value
Block	6.72		53.28	0.000
Linear	68.22		121.23	0.000
Quadratic	18.10		38.61	0.000
2-way interaction	7.02		4.08	0.039
Total model	99.97	99.90	55.78	0.000

using esterified BPF. This is obvious from Fig. 6 where the contours are somewhat curve representing a good interaction between the variables. The 3D plots showed that when other parameters are kept constant, high percentage sorption would be achieved at high temperature and dosage.

3.9. ANN modeling

The neural toolbox (nftool) of MATLAB 2015 a software was used in the artificial neural network analysis. Iteration method involving trial and error method was used to determine the optimal number of neurons in the hidden layer. Nine neurons were obtained as the optimum based on the lowest mean square error. Consequently, the topology of the optimum neural network architecture was 5–9-1 corresponding to five input neurons (representing the five input variables), nine neurons in the hidden layer and one output neuron (representing the percentage of oil removal).

Levenberg-Marquardt (LM) type of Multi-Layer Perceptron (MLP) was used as the training algorithm because its training stops simultaneously when generalization stops improving. The regression plots of training, testing, validation and overall datasets were given in Fig. 7. Correlation coefficients (R^2) of 0.9944, 0.9890, and 0.9928 with mean square error (MSE) values of 1.813×10^{-5}, 2.556×10^{-5} and 2.746×10^{-5} were obtained for the training, validation, and

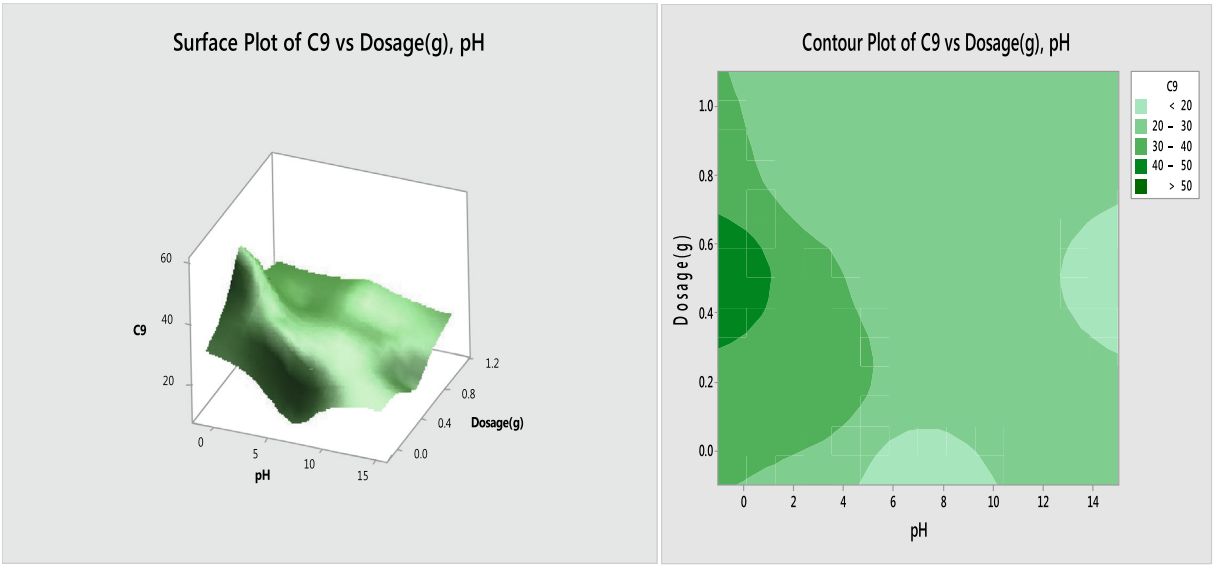

Fig. 5 Response surface and contour plots for the effect of pH and dosage on soption of oil by esterified BPF.

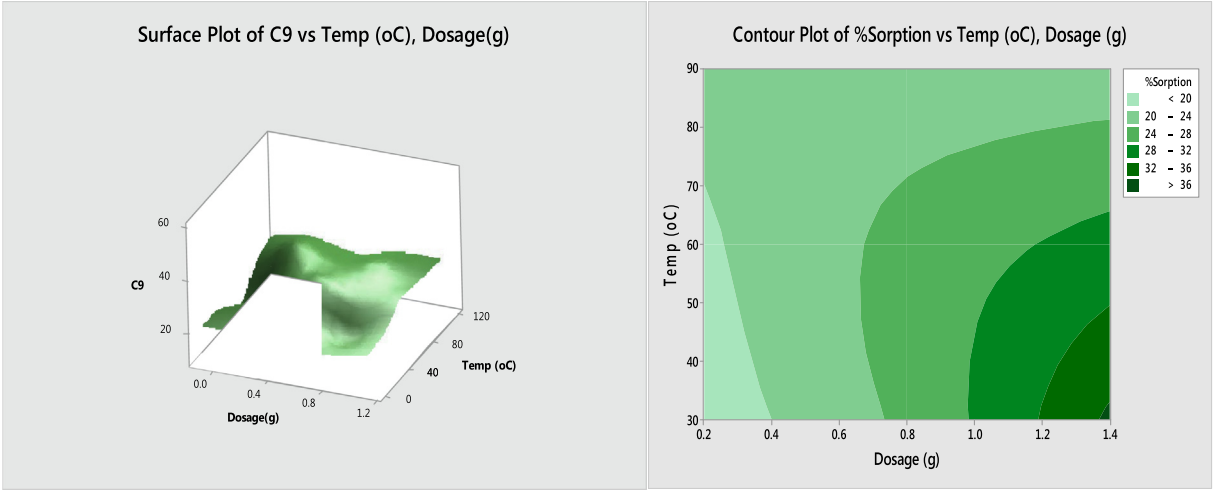

Fig. 6 Response surface and contour plots for the effect of dosage and temperature on soption of oil by esterified BPF.

testing respectively. These values suggested acceptable percentage oil removal by the ANN modeling which was confirmed by the high R^2 of the overall data set ($R^2 = 0.9934$).

The reliability of any model is an important factor in determining its acceptability. The performance validation plot was used to test for the reliability of the proposed ANN model. It showed the variation of the MSE with the required number of epochs for the optimal ANN architecture. The plot indicated a maximum of 9 epochs with the lowest validation mean square error of 2.55×10^{-5} obtained at the 8th epoch after which the training and validation curves were almost interwoven. The test curve decreased significantly after the 8th epoch showing that there was no over fitting in the data fragmentation (Onu et al., 2022; Azari et al., 2019; Dil et al., 2016).

3.10. ANFIS modeling

The ANFIS tool box (anfisedit) of MATLAB 2015a version was utilized for the ANFIS modeling of the oil removal process. The membership function (MF) used was gauss2mf which aided in predicting accurate result at a relatively small-time interval. The ANFIS modeling utilized the same number of data sets used in ANN.

The dataset was first divided into training, testing and checking with 80, 26, and 26 datasets respectively. The checking data was used to mitigate over-fitting and improve model generation (Kassema et al., 2017). The analysis of the ANFIS training, testing and checking gave R^2 of 0.9945, 0.9927, and 0.9912 with MSE of 4.27×10^{-3}, 5.21×10^{-3}, and

4.85×10^{-2} respectively. The low MSE values obtained suggested there was no over-fitting in the ANFIS training process and asserted that the ANFIS model was significant in modeling and predicting the percentage of oil removal. The major merit of the ANFIS is in achieving minimum error with the aid of fuzzy controllers enhanced with self-learning abilities (Onu et al., 2021, 2022).

The analysis of the overall data set was carried out using 45 epoch iterations at error tolerance of 0 with hybrid optimization as the fuzzy inference system (FIS) optimization method. Fig. 8 showed a significant correlation between the training data and the FIS output. This produced a small training MSE of 4.617×10^{-3} which stabilized at the 5th epoch. The R^2 of the overall data set was 0.999 which confirmed the suitability of the ANFIS model in modeling the percentage removal of oil via adsorption process.

RSM, ANN, and ANFIS models were comparatively evaluated based on the statistical analysis of their predicted percentage oil removal in Table 12. The result showed that the R^2 of the models were relatively similar with values of about 0.999 + 0.006. This implied that the three models gave adequate model predictions of the oil removal. Further statistical indices revealed the same similarity in the three models. RSM model seems to have marginally performed better than the ANN and the ANFIS models. Though many authors have reported on the superiority of ANN and ANFIS models over RSM model however, RSM have been reported to be better in modeling the design parameters for a V-perforated baffle and in modeling the parameters in potato drying (Sunil, 2015; Elijah et al., 2020).

3.11. Model comparison

Prediction between the three tools ANFIS, ANN, and RSM models were studied and verified as shown in Table 13. The difference between the experimental and the models' predictions values were simulated as the residuals. It was noticed that the three models gave a very low residuals as expected. The maximum negative and positive residuals were −0.001 and 0.6 as observed in ANN and ANFIS models respectively. Nev-

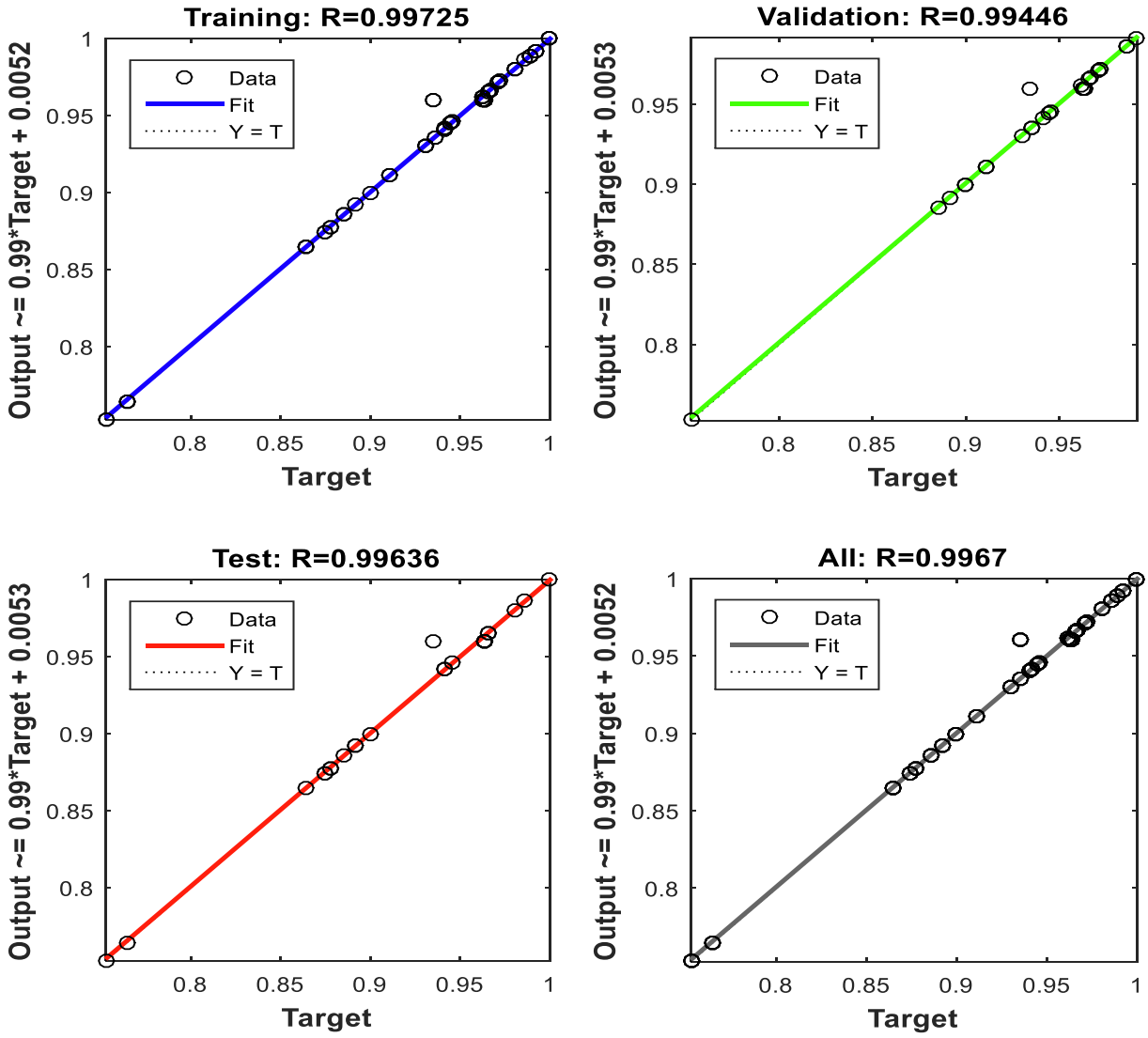

Fig. 7 ANN plots of training, validation, testing and overall data sets.

Fig. 8 ANFIS training and FIS output plot.

Table 12 Statistical analysis of the models.

Error indices	RSM	ANN	ANFIS
R^2	0.9996	0.9990	0.9994
SSE	0.3258	0.9938	0.8965
MPSED	0.00122	0.0021	0.00197
ARE	0.00094	0.000877	0.000519
HYBRID	0.00013	0.000396	0.000353
RMSE	0.00122	0.0021	0.00197

ertheless, RSM seems to be superior in performance because it has the maximum correlation coefficient of 0.9996. Thus, RSM was considered the most efficient model in predicting the oil removal followed by ANN (R^2 = 0.9990) and ANFIS (R^2 = 0.9994) models as evident in error indices in Table 12.

3.12. The optimum conditions and model validation

In furtherance to equation (14), the perfect conditions for the % of oil removed by BPF sample with respect to the proposed model equation were 100 °C, 0.2 g/100 cm^3, 1.5 g, 2 and 75 mins for temperature, oil concentration, adsorbent dosage, pH and time. At these conditions, the theoretical % of oil removed is 94.05% as evident in Table 9.

Validated % of oil removed by experiment is 95.21%. This was carried out by executing three independent experiments and taking the average value. Validity of the model was established by nearness of the validated and predicted % of oil removed. Chinonye et al., 2018; Nwabanne et al., 2017; Naghan et al., 2015; Onwu et al.2019a reported similar results for the optimization of crude oil adsorption using Kola nut shell and Ogbono shell . Their obtained optimum percentages were 76.32% and 88.57% respectively.

Table 13 Models' comparison for ANFIS, ANN and RSM models.

S/N	Temp (oC)	Oil/water (g/100 cm^3)	Sorbent dosage (g)	pH	Time (min)	Exp	Models' oil removal (%)			residuals		
							RSM	ANN	ANFIS	RSM	ANN	ANFIS
1	60	0.6	0.9	14	45	92.2	92.462	92.1999	92.2001	−0.262	0.0001	−0.0001
2	60	−0.2	0.9	6	45	83.31	83.219	83.3095	83.3101	0.091	0.0005	−0.0001
3	60	0.6	0.9	−2	45	90.5	90.226	90.4999	90.5001	0.274	0.0001	−0.0001
4	140	0.6	0.9	6	45	88.55	88.627	88.5495	88.5501	−0.077	0.0005	−0.0001
5	60	0.6	0.9	6	−15	71.89	71.801	71.8898	71.8901	0.089	0.0002	−0.0001
6	60	1.4	0.9	6	45	91.46	91.539	91.4597	91.4601	−0.079	0.0003	−0.0001
7	60	0.6	0.9	6	45	87.93	87.99	87.3076	87.9238	−0.06	0.6224	0.0062
8	−20	0.6	0.9	6	45	93.02	92.931	93.0192	93.0201	0.089	0.0008	−0.0001
9	60	0.6	2.1	6	45	84.62	84.507	84.6197	84.6201	0.113	0.0003	−1E-04
10	60	0.6	−0.3	6	45	81.32	81.421	81.3198	81.3201	−0.101	0.0002	−0.0001
11	60	0.6	0.9	6	105	82.53	82.607	82.5299	82.5301	−0.077	0.0001	−0.0001
12	20	0.2	1.5	2	15	88.5	88.66	88.4998	88.4997	−0.16	0.0002	0.0003
13	60	0.6	0.9	6	45	90.65	90.615	90.3076	90.2386	0.035	0.3424	0.4114
14	100	0.2	1.5	10	15	82.26	82.244	82.2601	82.2598	0.016	−1E-04	0.0002
15	20	1	0.3	2	15	90.92	90.984	90.9198	90.9197	−0.064	0.0002	0.0003
16	20	1	0.3	10	75	90.83	90.718	90.8294	90.8298	0.112	0.0006	0.0002
17	100	1	1.5	2	15	87.51	87.585	87.5099	87.5097	−0.075	0.0001	0.0003
18	20	1	1.5	2	75	92.74	92.815	92.7397	92.7398	−0.075	0.0003	0.0002

(*continued on next page*)

Table 13 (*continued*)

S/N	Temp (oC)	Oil/water (g/100 cm^3)	Sorbent dosage (g)	pH	Time (min)	Exp	Models' oil removal (%)			residuals		
							RSM	ANN	ANFIS	RSM	ANN	ANFIS
19	60	0.6	0.9	6	45	90.65	90.615	90.3076	90.2386	0.035	0.3424	0.4114
20	20	0.2	0.3	2	75	83.9	83.965	83.8997	83.8999	−0.065	0.0003	0.0001
21	100	1	0.3	10	15	85.68	85.568	85.68	85.6798	0.112	0	0.0002
22	100	0.2	1.5	2	75	90.91	90.986	90.9099	90.9097	−0.076	0.0001	0.0003
23	20	0.2	0.3	10	15	88.89	88.862	88.8899	88.8897	0.028	0.0001	0.0003
24	60	0.6	0.9	6	45	90.55	90.615	90.3076	90.2386	−0.065	0.2424	0.3114
25	100	0.2	0.3	10	75	93.31	93.199	93.3097	93.3096	0.111	0.0003	0.0004
26	100	1	0.3	2	75	94.07	94.05	94.0694	94.0697	0.02	0.0006	0.0003
27	60	0.6	0.9	6	45	90.6	90.615	90.3076	90.2386	−0.015	0.2924	0.3614
28	20	0.2	1.5	10	75	88.98	88.964	88.9794	88.9798	0.016	0.0006	0.0002
29	20	1	1.5	10	15	88.02	88.003	88.0201	88.0198	0.017	−0.0001	0.0002
30	60	0.6	0.9	6	45	90.65	90.615	90.3076	90.2386	0.035	0.3424	0.4114
31	100	1	1.5	10	75	91.38	91.28	91.3793	91.3798	0.1	0.0007	0.0002
32	100	0.2	0.3	2	15	70.78	70.845	70.7797	70.78	−0.065	0.0003	0
33	60	0.6	0.9	6	45	90.64	90.615	90.3076	90.2386	0.025	0.3324	0.4014

Table 14 Relationships in comparison with other works existing in literature.

Adsorbents	Removal capacity (qe) (mg/g)	Time (mins)	Amount of adsorbate (g/l)	References
Activated Kola nut shell	28.8	60	0.3	Chinonye et al., 2018
HCl activated cassava peels	24.30	50	0.3	Thompson et al., 2020
Activated Mosambi peels	38.9	60	0.5	Ladhe et al., 2011
Commercial Zeolite	55.30	50	0.2	Naema et al., 2014
Esterified BPF	49.33	50	0.2	This present study

3.13. Comparison between the present studies and prior researches in the similar field

In order to buttress the validity and efficacy of BPF in removing layers of oil from solvent, the performance was successfully compared with the existing ones as well as commercial zeolite as standard (see Table 14). In this context, adsorption capacities at a specified period of time were adopted as key performance index. The adsorption capacity obtained can be seen comparable to the zeolite as evident in the report by Naema et al., 2014. The unique observation about the present study can be linked to relatively high adsorption capacity obtained at a very minimal time. The adsorption capacity seems to have fared better than another adsorbent produced from similar biomass (see Table 14). Consequent upon this conviction, we arrived at a conclusion that the BPF is a good adsorbent with capacity comparable to the standard; even better than many and most importantly, the raw materials for the production is available at no cost.

4. Conclusion

The surface area of the Banana peels fibre as observed in the context increased from 295.6 to 556.8 cm^2/g after esterification with stearic acid. The removal of oil was optimal at 0.2/100 cm^3 with 98.2% of oil adsorbed. Error analysis proved that sorption of oil layers onto esterified BPF fitted well with Langmuir isotherm model. After thorough analysis using machine learning approach, the prediction modelling with RSM, ANN and ANFIS indicated efficient modeling of the percentage oil removal process as the experimental values were similar to the predictions of three models. The correlation coefficient of the three models were ≥ 0.999. The optimal performing process parameter revealed by the RSM was 100 °C, 0.2 g/100 cm^3, 1.5 g, 2 and 75 mins for temperature, oil concentration, adsorbent dosage, pH and time. At these conditions, the theoretical % of oil removed is 94.05 which was experimentally validated as 95.21.

Declaration of Competing Interest

The authors declare that they have no known competing financial interests or personal relationships that could have appeared to influence the work reported in this paper.

References

Ahmad, T., Danish, M., 2018. Prospects of banana waste utilization in wastewater treatment: A review. J. Environ. Manage. 206, 330–348.

Ahmadi, E., Kakavandi, B., Azari, A., Izanloo, H., Gharibi, H., Mahvi, A.H., Javid, A., Hashemi, S.Y., 2016. The performance of mesoporous magnetite zeolite nanocomposite in removing dimethyl phthalate from aquatic environments. Desalin. Water Treat. https://doi.org/10.1080/19443994.2016.1178174.

Akpomie, K.G., Conradie, J., 2020. Banana peel as a biosorbent for the decontamination of water pollutants. A review. Environ. Chem. Lett. https://doi.org/10.1007/s10311-020-00995-x.

Albert, C.A., Asadu, C.O., Onoh, M.I., Azubuike, K.A., 2016. Kinetics and Isotherm Studieson Divalent Lead Ions Adsorption by Zeolite Solution. Int. J. Novel Res. Eng. Sci. 31, 49–61.

Alvarez-López, C., Rojas, O.J., Rojano, B., Gañán, P., 2014. Development of self-bonded fiberboards from fiber of leaf plantain: Effect of water and organic extractives removal. Bio Resources 10 (1). https://doi.org/10.15376/biores.10.1.672-683.

Annunciado, T.R., Sydenstricker, T.H.D., Anuco, S.C., 2005. Experimental Investigation of Various Vegetable Fibers as Sorbent Materials for Oil Spills Marine Pollution. Bulletin 50, 13040–13046.

Arivoli, S., Hema, M., Martin, P.D., 2019. Adsorption of malachite green onto carbon Prepared from Borassus bark. Arabian J. Sci. Eng. 34 (2A), 31–43.

Asadu, C.O., Egbuna, S.O., Ejikeme, P.C.N., 2018b. Survey on kinetic decomposition of organic matter and bio-fertilizer synthesis by composting sawdust, vegetable waste and sewage sludge. Journal of the Chinese Advanced Materials.

Asadu, C.O., Ezema, C.A., Onu, C.E., Ogbodo, N.O., Maxwell, O.I., Ugwele, O.F., Chukwuebuka, A.S., Onah, T.O., Nwakwasi, E.G., Sunday, I.S., Ezeh, E.M., 2022. Equilibrium isotherm modelling and optimization of oil layer removal from surface water by organic acid grafted plantain pseudo stem fiber. Case Studies in Chemical and Environmental Engineering 5 (100194), 1–12. https://doi.org/10.1016/j.cscee.2022.100194.

Asadu, C.O., Egbuna, S.O., Chime, T.O., Eze, C.N., Kevin, D., Mbah, G.O., Ezema, A.C., 2019. Survey on solid wastes management by composting: Optimization of key process parameters for biofertilizer synthesis from agro wastes using response surface methodology (RSM). Artificial Intell. Agric. 3, 52–56. https://doi.org/10.1016/j.aiia.2019.12.002.

Asadu, C.O., Anthony, E.C., Elijah, O.C., Ike, I.S., Onoghwarite, O. E., Okwudili, U.E., 2021b. Development of an adsorbent for the remediation of crude oil polluted water using stearic acid grafted coconut husk (Cocos nucifera) composite. Appl. Surface Sci. Adv. 6.

Asadu, Christian O., Elijah, O.C., Ogbodo, N.O., Anthony, E.C., Onyejiuwa, C.T., Onoh, M.I., Ike, I.S., Onoghwarite, O.E., Chukwuebuka, A.S., 2021a. Treatment of crude oil polluted water using stearic acid grafted mango seed shell (Mangifera indica) composite. Current Res. Green Sustainable Chem. 4. https://doi.org/10.1016/j.crgsc.2021.100169.

Asadu, C.O., Onoh, M.I., Albert, C.A., 2018a. Equilibrium Isotherm Studies on the Adsorption of Malachite Green and Lead Ion from Aqueous Solution Using Locally Activated Ugwaka Clay (Black Clay). Arch. Curr. Res. Int. 12 (2), 1–11. https://doi.org/10.9734/ACRI/2018/39302. ISSN: 2454-7077.

Awual, M.R., Kobayashi, T., Miyazaki, Y., Motokawa, R., Shiwaku, H., Suzuki, S., Okamoto, Y., Yaita, T., 2013. Selective lanthanide sorption and mechanism using novel hybrid Lewis base (N-methyl-N-phenyl-1,10-phenanthroline-2-carboxamide) ligand modified adsorbent. J. Hazard. Mater. 252–253, 313–320.

Awual, M.R., Hasan, M.M., Eldesoky, G.E., Khaleque, M.A., Rahman, M.M., Naushad, M., 2016. Facile mercury detection and removal from aqueous media involving ligand impregnated conjugate nanomaterials. Chem. Eng. J. 290, 243–251.

Awual, M.R., Hasan, M.M., Rahman, M.M., Asiri, A.M., 2019a. Novel composite material for selective copper(II) detection and removal from aqueous media. J. Mol. Liquids 283, 772–780.

Awual, M.R., Hasan, M.M., Asiri, A.M., Rahman, M.M., 2019b. Cleaning the arsenic(V) contaminated water for safe-guarding the public health using novel composite material. Compos. Part B: Eng. 171, 294–301.

Ayotamuno, M.J., Kogbara, R.B., Ogafi, S.O.T., Probert, S.D., 2006. Bioremediation of a Crude Oil Polluted Agricultural-Soil at Port-Harcourt. Nigeria J. Appl. Energy 83, 1249–1257.

Azari, A., Mahmoudian, M.H., Niari, M.H., Eş, I., Dehganifard, E., Kiani, A., Javid, A., Azari, H., Fakhri, Y., Khaneghah, A.M., 2019. Rapid and efficient ultrasonic assisted adsorption of diethyl phthalate onto $Fe^{II}Fe_2^{III}O_4$@GO: ANN-GA and RSM-DF modeling, isotherm, kinetic and mechanism study. Micro Molecule J. 150. https://doi.org/10.1016/j.microc.2019.104144.

Baars, B.J., 2002. The wreckage of the oil tanker 'Erika'-human health risk assessment of beach cleaning, sunbathing and swimming. Toxicol. Lett. 128 (1–3), 55–68.

Babaei, A.A., Khataee, A., Ahmadpour, E., Sheydaei, M., Kakavandi, B., Alaee, Z., 2016. Optimization of cationic dye adsorption on activated spent tea: Equilibrium, kinetics, thermodynamic and artificial neural network modeling. Korean J. Chem. Eng. https://doi.org/10.1007/s11814-014-0334-6.

Bagheri, R., Ghaedi, M., Asfaram, A., Dil, E.A., Javadian, H., 2019. RSM-CCD design of malachite green adsorption onto activated carbon with multimodal pore size distribution prepared from *Amygdalus scoparia*: Kinetic and isotherm studies. Polyhedron 171, 464–472. https://doi.org/10.1016/j.poly.2019.07.037.

Bahman, N., Sina, F.A., 2018. Application of ANFIS, ANN, and logistic methods in estimating biogas production from spent mushroom compost (SMC). Resour. Conserv. Recycl. 133, 169–178. https://doi.org/10.1016/j.resconrec.2018.02.025.

Banerjee, S.S., Joshi, M.V., Jayaram, R.V., 2006. Treatment of oil spill by sorption Technique using fatty acid grafted sawdust. Chemosphere 64, 1026–1031.

Bansal, S., Arnim, V.V., Stegmaier, T., Planck, H., 2011. Effect of fibrous filter properties On the oil-in –water emulsion separation and filtration performance. J. Hazard. Mater 190 (1–3), 45–50.

Behnood, R., Anvaripour, B., Jaafarzadeh, N., Farasati, M., 2013. Application of natural sorbents in crude oil adsorption. Oil Gas Sci. Technol. J. 2 (4), 01–11.

Behnood, R., Anvaripour, B., Jaafarzadeh, N., Farasati, M., 2016. Oil spill sorption using Raw and acetylated sugarcane bagasse. J. Cent. South Univ. 23, 1618–1625. https://doi.org/10.1007/s11771016-3216-8.

Berizi, Z., Hashemi, S.Y., Hadi, M., Azari, A., Mahvi, A.H., 2016. The study of non-linear kinetics and adsorption isotherm models for Acid Red 18 from aqueous solutions by magnetite nanoparticles and magnetite nanoparticles modified by sodium alginate. Water Sci. Technol. 74 (5), 1235–1242. https://doi.org/10.2166/wst.2016.320.

Cadena, E.M., Ch, J.M., Vélez, R., Santa, J.F., Otálvaro, V.G., 2017. Natural Fibers from Plantain Pseudostem (Musa Paradisiaca) for Use in Fiber-ReinforcedComposites. J. Nat. Fibers. https://doi.org/10.1080/15440478.2016.1266295.

Cheenmatchaya, A., Kungwakunakorn, S., 2014. Preparation of Activated Carbon Derived From Rice Husk by simple Carbonization and Chemical Activation for Using as Gasoline Adsorbent. Int. J. Environ. Sci. Develop 5 (2), 21–33.

Chinonye, O.E., Oluchukwu, A.C., Elijah, O.C., 2018. Statistical analysis for orange G adsorption using kola nut shell activated carbon. J. Chinese Adv. Mater. Soc. https://doi.org/10.1080/22243682.2018.1534607.

Dil, E.A., Ghaedi, M., Ghezelbash, G.R., Asfaram, A., Ghaedi, A.M., Mehrabi, F., 2016. Modeling and optimization of Hg^{2+} ion biosorption by live yeast Yarrowia lipolytica 70562 from aqueous solutions under artificial neural network-genetic algorithm and response surface methodology: kinetic and equilibrium study. RSC Adv. 6, 54149–54161.

Dil, E.A., Ghaedi, M., Asfaram, A., Mehrabi, F., Bazrafshan, A.A., Tayebi, L., 2019a. Synthesis and application of Ce-doped TiO_2 nanoparticles loaded on activated carbon for ultrasound-assisted adsorption of Basic Red 46 dye. Ultrasonic Sonochemistry 58. https://doi.org/10.1016/j.ultsonch.2019.104702.

Dil, E.A., Ghaedi, M., Asfaram, A., Mehrabi, F., Sadeghfar, F., 2019b. Efficient adsorption of Azure B onto CNTs/Zn:ZnO@-Ni2P-NCs from aqueous solution in the presence of ultrasound wave based on multivariate optimization. J. Ind. Eng. Chem. 74 (25), 55–62. https://doi.org/10.1016/j.jiec.2018.12.050.

Egbuna, S.O., Onwubiko, D.C., Asadu, C.O., 2019a. Comparative Studies and Optimization of the Process Factors for the extraction of Beta-carotene from Palm oil and Soybean oil by Solvent extraction. J. Eng. Res. Reports. 8 (2), 1–16.

Egbuna, S.O., Onwubiko, D.C., Asadu, C.O., 2019b. Kinetics and Thermodynamic Studies of Beta Carotene Extraction from Palm Oil by Solvent Extraction. J. Mater. Sci. Res. Rev. 4 (2), 1–13.

Elijah, O.C., Igbokwe, P.K., Nwabanne, J.T., Nwanjinka, O.C., Ohale, P.E., 2020. Evaluation of optimization techniques in predicting optimum moisture content reduction in drying potato slices. Artif. Intell. Agric. 4, 39–47. https://doi.org/10.1016/j.aiia.2020.04.001.

Ezedinma, Henry C., Nwabanne, Jospeh T., Onu Chijioke, E., Nwajinka, C.O., 2021. Optimum Process Parameters and Thermal Properties of Moisture Content Reduction in Water Yam Drying. Asian Journal of Chemical Sciences 9 (4), 44–54. https://doi.org/10.9734/AJOCS/2021/v9i419080.

Ezenwa, O., Asadu, C.O., Agaba, A., 2019. Optimization and Kinetic Modeling of the Removal of Lead from Enugu Coal by Acid Leaching. J. Energy Res. Reviews 3 (1), 1–13. https://doi.org/10.9734/jenrr/2019/v3i130090.

Fazal, A., Rafique, U., 2013. Severance of lead by acetylated and esterified spent camellia sinensis Powder. Am. J. Environ. Eng. 3 (6), 288–296. https://doi.org/10.5923/j.ajee.20130306.04.

Gholamhossein, S., Seyed, A.S., Nedasadat, S.A., 2016. Evaluation of the response surface and hybrid artificial neural network-genetic algorithm methodologies to determine extraction yield of ferulago angulata through supercritical fluid. J. Taiwan Ins. Chem. Eng. 60, 165–173. https://doi.org/10.1016/j.jtice.2015.11.003.

Gwendoline, F., 2010. The Effects of Oil Spills of Aquatic Life and Environments. J. Sci. Natural 2 (4), 23–30.

Happi-Emaga, T., Bindelle, J., Agneesens, R., Buldgen, A., Wathelet, B., Paquot, M., 2011. Ripening influences banana and plantain peels composition and energy content. Tropical Animal Health Prod. 43, 171–177. https://doi.org/10.1007/s11250-010-9671-6.

Hikmat, N.A., Qassim, B.B., Khethi, M.T., 2014. "Thermodynamic and Kinetic Studies of Lead Adsorption from Aquesous Solution onto Petiole and Fiber of Palm Tree. Am. J. Chem. 4 (4), 116–124, p-ISSN: 2165-8749 e-ISSN: 2165-8781.

Kassema, Y., Hüseyin, C., Engin, E., 2017. Adaptive neuro-fuzzy inference system (ANFIS) and response surface methodology (RSM) prediction of biodiesel dynamic viscosity at 313 K. Procedia Comput. Sci. 120, 521–528. https://doi.org/10.1016/j.procs.2017.11.274.

Karimi, F., Rafiee, S., Taheri, G.A., Karimi, M., 2012. Optimization of an air drying process for Artemisia absinthium leaves using response surface and artificial neural network models. J. Taiwan Inst. Chem. Eng. 43, 29–39. https://doi.org/10.1016/j.jtice.2011.04.005.

Kharoune, M., Pauss, A., LebeaultJ, M., 2001. Aerobic Biodegradation of an Oxygenates Mixture: ETBE, MTBE and TAME in an Upflow Fixed-bed Reactor. Water Resour. 35 (7), 1665–1674.

Kudaybergenov, K.K., Ongarbayev, E.K., Mansurov, Z.A., 2015. Oil sorption by Heat- Treated rice husks. J. Petrol. Environ. Biotechnol. 6, 5–13.

Kumar, K.V., 2006. Comparative analysis of linear and non-linear method of estimating the sorption isotherm parameters for malachite green onto activated carbon. J. Hazard. Mater. 136 (2), 197–202.

Ladhe, U.V., Wankhede, S.K., Patil, V.T., Patil, P.R., 2011. Adsorption of eriochrome blackT from aqueous solutions on activated carbon prepared from mosambi peel. J. Appl. Sci. Environ. Sanit. 6 (2), 149–154.

Meybodi, A.A., Ebadi, A.S., Shafiei, S., Khataee, A., Rostampour, M., 2015. Modeling and optimization of antidepressant drug Fluoxetine removal in aqueous media by ozone/H2O2 process: Comparison of central composite design and artificial neural network approaches. J. Taiwan Inst. Chem. Eng. 48. https://doi.org/10.1016/j.jtice.2014.10.022.

Moghaddam, M.H., Nabizadeh, R., Dehghani, M.H., Akbarpour, B., Azari, A., Yousefi, M., 2019. Performance investigation of Zeolitic Imidazolate Framework-8 (ZIF-8) in the removal of trichloroethylene from aqueous solutions. Microchem. J. 150, 104185.

Mourabet, M.E., Rhilassi, A., Bennani-Ziatni, M., Taitai, A., 2014. Comparative Study of artificial neural network and response surface methodology for modelling and optimization the adsorption capacity of fluoride onto apatitic tricalcium phosphate. Universal J. Appl. Math. 2 (2), 84–91. https://doi.org/10.13189/ujam.2014.020202.

Naghan, D.J., Azari, A., Mirzaei, N., Velayati, A., Tapouk, F.A., Adabi, S., Pirsaheb, M., Sharafi, K., 2015. Parameters effecting on photocatalytic degradation of the phenol from aqueous solutions in the presence of ZnO nanocatalyst under irradiation of UV-C light. Bulgarian. Chem. Commun. 47, 14–18. Special Edition D.

Nestor, T., Natalia, M., Fabiana, M., Javier, P., Carina, P., Tomas, Phenol, C., 2004. Adsorption onto powdered and granular activated carbon, prepared from eucalyptus wood. J. Colloid Interface Sci. 279, 357–363.

Nnaemeka, I.C., Samuel, E., Maxwell, O., AsaduChristain, O.C., 2021. Optimization and kinetic studies for enzymatic hydrolysis and fermentation of colocynthis vulgaris Shrad seeds shell for bioethanol production. J. Bioresources Bioprod. 6, 45–64.

Nwabanne, J.T., Okpe, E.C., Asadu, C.O., Onu, C.E., 2017. Application of Response Surface Methodology in Phenol Red Adsorption Using Kola Nut (Colaacuminata) Shell Activated Carbon. Int. Res. J. Pure Appl. Chem. 15 (4), 1–14.

Nwabanne, J.T., Okpe, E.C., Asadu, C.O., Onu, C., E,, 2018. Sorption Studies of Dyestuffs on Low-cost Adsorbent. Asian J. Phys. Chem. Sci. 5 (3), 1–19.

Nwobasi, V.N., Igbokwe, P.K., Onu, C.E., 2022. Optimization of Acid Activated Ngbo Clay Catalysts in Esterification Reaction Using Response Surface Methodology. Asian Journal of Physical and Chemical Sciences 10 (1), 11–27. https://doi.org/10.9734/AJOPACS/2022/v10i130147.

Ogbodo, N.O., Asadu, C.O., Ezema, C.A., Onoh, M.I., Elijah, O.C., Ike, I.S., Onoghwarite, O.E., 2021. Preparation and Characterization of activated carbon from agricultural waste (Musa-paradisiacapeels) for the remediation of crude oil contaminated water. J. Hazard. Mater. Adv. https://doi.org/10.1016/j.hazadv.2021.100010.

Okafor, E., Ihueze, C., Nwigbo, S., 2012. Optimization of hardness strengths response of plantain fibres reinforced polyester matrix composites (PFRP) applying Taguchi robust design. Int. J. Eng.-Trans. A: Basics 26 (1), 1.

Olufemi, B.A., Jimoda, L.A., Agbodike, N.F., 2014. Adsorption of Crude Oilusing Meshed Corncobs. Asian J. Appl. Sci. Eng. 3, 63–75.

Omar, H.A., 2012. Adsorptive removal of phenol from aqueous solution using natural immobilized Chitin by Diathiazone. New York Science J. 5 (8), 1–9.

Onu, C.E., Nwabanne, J.T., Ohale, P.E., Asadu, C.O., 2021. Comparative analysis of RSM, ANN and ANFIS and the mechanistic modeling in eriochrome black-T dye adsorption using modified clay. South Afr. J. Chem. Eng. 36, 24–42.

Onu, C.E., Igbokwe, P.K., Nwabanne, J.T., Ohale, P.E., 2022. ANFIS, ANN, and RSM modeling of moisture content reduction of cocoyam slices. J. Food Process. Preserv. 46 (1), 1–19. https://doi.org/10.1111/jfpp.16032. e16032.

Onwu, D.O., Ogbodo, O.N., Ogbodo, N.C., Chime, T.O., Udeh, B.C., Egbuna, S.O., Onoh, M.I., Asadu, C.O., 2019a. Application of Esterified Ogbono Shell Activated Biomass as an Effective Adsorbent in the Removal of Crude Oil layer from Polluting Water Surface. J. Appl. Sci. Environ. Manage. 23 (9), 1739–1746.

Onwu, D.O., Nick, O., Cordelia, O.N., Asadu, C.O., Maxwell, O.I., 2019b. Optimization of Process Parameters for the Treatment of Crude Oil Spill Polluting Water Surface by Sorption Technique Using Fatty Acid Grafted Ogbono Shell as a Sorbent. J. Mater. Sci. Res. Rev. 3 (3), 1–12.

Onyekwelu, I.U., Nwabanne, J.T., Onu, C.E., 2021. Characterization and Optimization of Biodiesel Produced from Palm Oil Using Acidified Clay Heterogeneous Catalyst. Asian J. Appl. Chem. Res 8 (3), 9–23. https://doi.org/10.9734/AJACR/2021/v8i330192.

Ozçimen, D., 2012. An Approach to the Characterization of Biochar and Bio-Oil. Bioengineering Department Yildiz Technical University, Turkey.

Paulauskiene, T., Jucike, I., Juseenko, N., Baziuke, D., 2014. The use of natural sorbents For spilled crude oil and diesel cleanup from the water surface. 2014.

Pelissari, F.M., Amaral-Sobral, P.J., Menegalli, F.C., 2014. Isolation and characterization of cellulose nanofibers from banana peels. Cellulose 21, 417–432. https://doi.org/10.1007/s10570-013-0138-6.

Pragnesh, N.D., Satindar, K., Ekta, K., 2011. Removal of eriochrome black –T by Adsorption onto eucalyptus bark using green technology. Indian J. Chem. Technol. 18, 53–60.

Rahman, N., Haseen, U., 2014. Equilibrium Modeling, Kinetic, and Thermodynamic Studies on Adsorption of Pb(II) by a Hybrid Inorganic-Organic Material: Polyacrylamide Zirconium(IV) Iodate. Ind. Eng. Chem. Res 53 (19), 8198–8207. https://doi.org/10.1021/ie500139k.

Rahman, N., Nasir, M., Alothman, A.A., Al-Enizi, A.M., Ubaidullah, M., Shaikh, S.F., 2021a. Synthesis of 2-mercaptopropionic acid/hydrous zirconium oxide composite and its application for removal of Pb(II) from water samples: Central composite design for optimization. J. King Saud Univ. – Sci. 33 (2). https://doi.org/10.1016/j.jksus.2020.101280.

Rahman, N., Raheem, A., 2022. Graphene oxide/Mg-Zn-Al layered double hydroxide for efficient removal of doxycycline from water: Taguchi approach for optimization. J. Mol. Liquid. 354. https://doi.org/10.1016/j.molliq.2022.118899.

Rahman, N., Varshney, P., Nasir, M., 2021b. Synthesis and characterization of polydopamine/hydrous zirconium oxide composite and its efficiency for the removal of uranium (VI) from water. Environ. Nanotechnol. Monit. Manage. 15, 100458.

Rashmi, S., Bhattacharya, B., 2003. Adsorption-coagulation for the decolorisation of Textile dye solutions. Water Qual. Res. J. Canada 38 (3), 553–562.

Reza, B., Bagher, A., Nematollah, J.H.F., Masoumeh, F., 2013. Application of Natural Sorbents in Crude Oil Absorption. Iranian J. Oil Gas Sci. Technol. 2, 01–11.

Sheela Tand Arthoba, N., 2012. Kinetics and thermodynamics of cadmium and lead ions adsorption on NiO nanoparticles. Chem. Eng. J. 191, 123–131.

Suidan, M.T., Esperanza, M., Zein, P., McCauley, R.C., Brenner, A. D., 2005. Challenges in Biodegradation of Trace Organic Contaminants-Gasoline Oxygenates and Sex Hormones. Water Environ. Res. 77 (1), 4–11.

Sunil, C., 2015. ANN and RSM approach for modeling and optimization of designing parameters for a V down perforated baffle roughened rectangular channel. Alex. Eng. J. 54, 429–446.

Thompson, Chime O., Ndukwe, Agu O., Asadu, Christian O., 2020. Application of activated biomass waste as an adsorbent for the removal of lead (II) ion from wastewater. Emerging Contaminants 6, 259–267.

Ugwele, F.O., Aninwede, C.S., Chime, T.O., Asadu, C.O., Ike, S.I., 2020. Application of Response Surface Methodology in Optimizing the Process Conditions for the Regeneration of Used Mobil Oil using different kinds of Acids. Heliyon J. https://doi.org/10.1016/j.heliyon.2020.e05062.

Verma, V.K., Mishra, A.K., 2010. Kinetic and isotherm modeling of adsorption of dyes Onto rice husk carbon. Global Nest J. 10 (10), 1–7.

Vigneswaran, C., Pavithra, V., Gayathri, V., Mythili, K., 2015. Banana fiber: Scope and value added product development. J. Textile Apparel, Technol. Manage. 9 (2), 1–7.

Yang, G., Zhang, L., Sun, X., Jing, W., 2006. Photochemical Degradation of Crude Oil in Sea Water. Chinese J. Oceanol. Limnol. 24 (3), 264–269.